ELSEVIER

Palaeogeography, Palaeoclimatology, Palaeoecology 198 (2003) 145–168

PALAEO

www.elsevier.com/locate/palaeo

Magnetostratigraphic calibration of Southern Ocean diatom datums from the Eocene–Oligocene of Kerguelen Plateau (Ocean Drilling Program sites 744 and 748)

Andrew P. Roberts [a,*], Simon J. Bicknell [a], Joanne Byatt [a], Steven M. Bohaty [b], Fabio Florindo [a,c], David M. Harwood [d]

[a] *School of Ocean and Earth Science, University of Southampton, Southampton Oceanography Centre, European Way, Southampton SO14 3ZH, UK*

[b] *Department of Earth Sciences, University of California, Santa Cruz, CA 95064, USA*

[c] *Istituto Nazionale di Geofisica e Vulcanologia, Via di Vigna Murata, 605, 00143 Rome, Italy*

[d] *Department of Geosciences, University of Nebraska, Lincoln, NE 68588-0340, USA*

Received 7 February 2002; accepted 3 March 2003

Abstract

Ocean Drilling Program holes 744A and 748B represent key sections for calibration of Southern Ocean Eocene–Oligocene biostratigraphic zonations. Sites 744 and 748 were above the carbonate compensation depth throughout this time interval and contain good planktonic foraminiferal, calcareous nannofossil, and diatom biostratigraphic records. In particular, the Southern Ocean diatom biostratigraphic zonation for the Oligocene critically hinges on calibration of these two holes. Previous low-resolution magnetostratigraphic studies at these sites were hampered by limited sampling and technical difficulties, which prompted our high-resolution reinvestigation of the magnetostratigraphy. Magnetic polarity zonations for holes 744A and 748B were constructed after inspection of vector component plots at 1-cm stratigraphic intervals from continuous u-channel measurements. The magnetizations are generally stable and a robust polarity stratigraphy has been obtained for both holes. The increased resolution of our study and identification of persistent secondary overprints, which were not recognised in previous studies, suggests that the previously published interpretations need to be revised. Our magnetostratigraphic interpretations for both holes are constrained by foraminiferal and calcareous nannofossil datums, as well as by Sr isotope ages. We have calibrated four diatom datums, which are synchronous at the two studied sites, to the geomagnetic polarity timescale, including the first occurrence (FO) of *Lisitzinia ornata* (27.8 Ma), the FO of *Rocella vigilans* var. B (27.8 Ma), the FO of *Cavitatus jouseanus* (30.9 Ma) and the FO of *Rhizosolenia oligocaenica* (33.8 Ma). The synchroneity of these datums suggests that diatom biostratigraphy has considerable potential for Palaeogene biostratigraphic correlation in the Southern Ocean. Although the ages of some datums are obscured by an unconformity in Hole 744A, our age model from Hole 748B suggests age estimates for the last common occurrence of *Rocella vigilans* var. A (~29.0 Ma), the FO of *Rocella vigilans* var. A (30.0 Ma) and the FO of *Rhizosolenia antarctica* (33.2 Ma). It should also be noted that the last occurrence of the calcareous nannofossil *Chiasmolithus altus* occurs in Chron C8r rather than C8n in our revised magnetostratigraphic interpretation, which indicates that this datum is not diachronous between low and mid

* Corresponding author. Tel.: +44-23-80593786; Fax: +44-23-80593059.
E-mail address: arob@mail.soc.soton.ac.uk (A.P. Roberts).

0031-0182/03/$ – see front matter
doi:10.1016/S0031-0182(03)00397-3

latitudes as had previously been suggested. Significant unconformities are documented in both holes, in the middle Oligocene and in the middle late Oligocene, respectively, which probably resulted from periods of enhanced circumpolar deep-water circulation.

Keywords: Eocene; Oligocene; Ocean Drilling Program; 744A; 748B; Kerguelen Plateau; Antarctica; magnetostratigraphy; biostratigraphy; diatoms; foraminifera; calcareous nannofossils

1. Introduction

Global cooling and development of the Antarctic ice sheets during the Palaeogene have been attributed to a number of mechanisms. These mechanisms include thermal isolation of Antarctica as a result of tectonic opening of oceanic gateways (Lawver et al., 1992), Tibetan Plateau uplift since the middle Eocene (Ruddiman and Kutzbach, 1989; Raymo and Ruddiman, 1992; Chung et al., 1998), Palaeogene uplift of the Transantarctic Mountains (Fitzgerald, 1992), changes in the concentration of radiatively important trace gases (particularly CO_2) in the atmosphere (Pearson and Palmer, 2000), and extraterrestrial impacts in the early middle Eocene and the late Eocene (Koeberl et al., 1996; Bottomley et al., 1997; Farley et al., 1998; Vonhof et al., 2000). The relative roles of these mechanisms have crucial importance for understanding changes in ocean circulation, carbon cycling, and biotic and climatic evolution during this period of global cooling, yet they are only vaguely understood.

Understanding the history of the Antarctic ice sheets during the Eocene–Oligocene transition requires direct stratigraphic records from ice-proximal high latitude sites. It is often difficult to extract high-resolution chronostratigraphic records from high latitude sedimentary archives because they usually contain numerous disconformities and microfossil preservation is often sporadic (e.g. Harwood et al., 1998; Roberts et al., 1998; Wilson et al., 1998, 2000; Florindo et al., 2001, 2003). In order to correctly interpret Antarctic margin records of environmental and climatic change, it is fundamental to optimise the chronostratigraphic value of these records by ensuring that biostratigraphic datums are as well calibrated as possible. This can only be achieved if clearly defined biostratigraphic zonations can be securely calibrated to a global chronostratigraphic framework, such as magnetostratigraphy, from more continuously deposited sites in the Southern Ocean. In particular, high latitude sites usually have poor carbonate preservation and siliceous microfossils are often more abundant than calcareous microfossils. Calibration of diatom datums is therefore particularly important for such coring localities.

The synchroneity of diatom events in the Palaeogene is largely untested in the Southern Ocean. In order to test for synchroneity, several conditions must be met, including: uniformity of taxonomic concepts between sites, stratigraphically continuous sections, high-quality palaeomagnetic data, good siliceous microfossil preservation and high sampling resolution. Ocean Drilling Program (ODP) sites 744 and 748 generally meet these requirements and provide good locations for testing the biostratigraphic value of diatom datums in the Southern Ocean. In this paper, we present new high-resolution magnetostratigraphic results from Eocene–Oligocene sediments recovered at sites 744 and 748 from the southern Kerguelen Plateau. The new data are used to constrain the published diatom biostratigraphy from these sites (Baldauf and Barron, 1991; Harwood and Maruyama, 1992). Sites 744 and 748 represent two of a small number of mid–southern latitude sites for which a magnetobiostratigraphic calibration is available. They therefore represent an important resource for constraining Eocene–Oligocene records from the Southern Ocean and Antarctic margin. Magnetostratigraphic results have been previously reported for sites 744 and 748 (Keating and Sakai, 1991; Inokuchi and Heider, 1992). However, problems

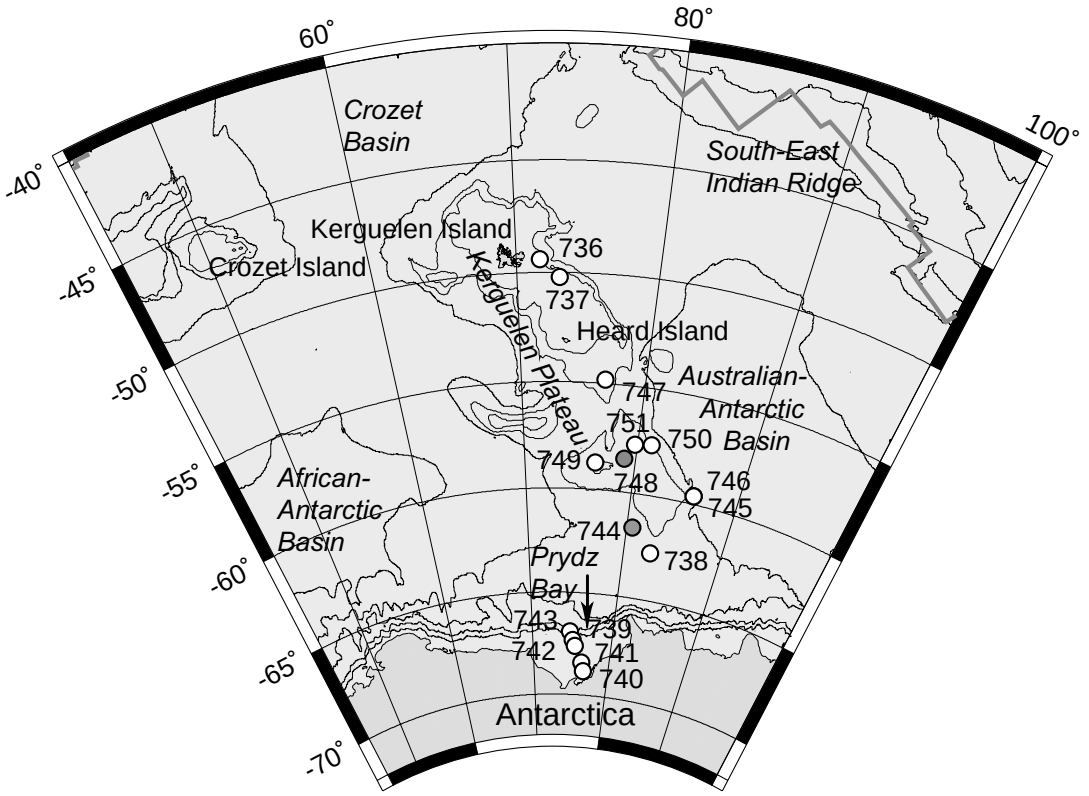

Fig. 1. Map of the Kerguelen Plateau and ODP sites drilled during ODP legs 119 and 120 (including Prydz Bay). Sites 744 and 748 (shaded dots) are from the southern Kerguelen Plateau. The bathymetric contour interval is 1000 m.

with the resolution and quality of these earlier studies suggested to us that, because of the importance of these sites to global chronostratigraphic compilations (e.g. Berggren et al., 1995), a more detailed study was warranted. For example, several comments by Keating and Sakai (1991) give cause for concern. First, faulty shipboard software meant that the background signal had been incorrectly computed during palaeomagnetic measurements, which cast doubt on the reliability of the results. Second, blanket alternating field (AF) demagnetization was carried out on all discrete samples at 15, 22.5 and 30 mT by Keating and Sakai (1991) for Hole 744A and only at 9 mT for half-core measurements by Inokuchi and Heider (1992) for Hole 748B. This treatment will give useful results if secondary overprints are removed at these maximum demagnetization levels. However, such abbreviated blanket demagnetization schemes are no longer considered acceptable for routine sample treatment (e.g. Opdyke and Channell, 1996), and stronger overprints, which can compromise magnetostratigraphic studies, are routinely reported from ODP cores (e.g. Stoking et al., 1993; Roberts et al., 1996; Fuller et al., 1998). Third, ODP sampling policy at the time of the initial studies prevented sampling of the cores at sufficient resolution to detect the complete polarity sequence. Relaxation of ODP sampling policy in the last few years has enabled us to collect continuous u-channel samples from these important sites to revise the earlier magnetobiostratigraphic calibrations for ODP holes 744A and 748B.

2. Geological setting and sampling

The Kerguelen Plateau lies in the Southern Indian Ocean (Fig. 1) and is one of the world's two

most voluminous large igneous provinces (Coffin and Eldholm, 1994). Igneous activity at the Kerguelen Plateau and the conjugate Broken Ridge, which is separated from the Kerguelen Plateau by the Southeast Indian Ridge, was probably related to the Mesozoic break-up of the Indian, Australian and Antarctic plates (Tikku and Cande, 2000; Gladczenko and Coffin, 2001). The elevation of the Kerguelen Plateau above the surrounding deep ocean basins (Fig. 1) results from upwelling of hot asthenospheric material associated with the Kerguelen hot spot (Gladczenko and Coffin, 2001). The Kerguelen Plateau contains well-developed sedimentary basins, which formed as a result of post-emplacement extension and rifting that culminated in the Eocene separation of Kerguelen Plateau and Broken Ridge (Munschy et al., 1992). These basins were drilled during ODP legs 119 and 120 to obtain records of the late Palaeogene northward expansion and subsequent fluctuations of Antarctic water masses. Site 744 was cored during ODP Leg 119 and Site 748 was cored during ODP Leg 120 (Barron et al., 1989; Schlich et al., 1989). These sites are located on the southern Kerguelen Plateau at water depths of 2308 and 1291 m, respectively (Fig. 1). ODP sites 744 and 748 lie 900 km south of the present-day Antarctic convergence and to the north of a constricted deep-water passage (>3500 m) that separates the Kerguelen Plateau from Antarctica (Fig. 1). This location would be expected to record erosive events associated with fluctuations of circumpolar deep water as it moved eastward around Antarctica. At these sites, Eocene–Oligocene sediments are exposed at shallow depths below the sea floor. It was therefore possible to recover thick sequences of unsilicified Palaeogene sediments using hydraulic piston coring. The sediments were deposited in a pelagic setting which is largely free of the considerable terrigenous influence observed on the Antarctic margin further south, such as at Prydz Bay (Barron et al., 1989; O'Brien et al., 2001). The presence of carbonate throughout the studied interval suggests that the sites were situated above the carbonate compensation depth (CCD) at least since the Eocene. The studied sediments are calcareous nannofossil oozes, with a minor, but well-preserved, biosiliceous component in the post-Eocene part of the record (e.g. Bohaty and Harwood, 2000). Siliceous microfossils are also present in middle and upper Eocene sediments from Hole 748B, but are generally not as well preserved as in the Oligocene.

Holes 744A and 748B were sampled at the ODP East Coast Repository at Lamont–Doherty Earth Observatory (LDEO) using 2 cm$\times$2 cm square cross-section plastic u-channel samples (up to 1.5 m in length). After shipment from LDEO, the samples were stored in a refrigerated room at the Southampton Oceanography Centre (SOC). Samples were taken from the archive halves of cores 12H–20H from Hole 744A (99.2–176.1 metres below sea floor (mbsf)) and from cores 9H–20H from Hole 748B (66.6–180.6 mbsf).

3. Methods

Palaeomagnetic measurements were made on u-channel samples with a narrow-access pass-through cryogenic magnetometer equipped with high-resolution pick-up coils. The Gaussian shape of the magnetometer response function means that measurements are smoothed over a stratigraphic interval of about 4.5 cm (Weeks et al., 1993). All measurements were made in the magnetically shielded palaeomagnetic laboratory at the SOC. The natural remanent magnetization (NRM) of the u-channel samples was subjected to stepwise AF demagnetization at applied fields of 10, 15, 20, 25, 30, 35, 40, 50, and 60 mT using an AF demagnetizer that is configured in-line with the cryogenic magnetometer. Higher fields were applied only when a significant part of the NRM remained after treatment at 60 mT. The NRM remaining at each demagnetization step was measured at 1-cm intervals along each section of core. Precise control on the position of the u-channel on the computer-controlled sample handling track means that vector component plots can be made for each measurement point throughout the studied stratigraphic interval. Vector component plots were, therefore, inspected at 1-cm intervals for all of the studied cores. If the

magnetization of the sediment was stable, the characteristic remanent magnetization (ChRM) was determined using principal component analysis (PCA) (Kirschvink, 1980) with a minimum of four data points at successive stepwise demagnetization levels. The quality of fit of a straight line to the ChRM component was quantified by determining the maximum angular deviation (MAD) for each measurement point (Kirschvink, 1980). Where possible, we report data at 1-cm stratigraphic intervals; however, it should be remembered that data points are only independent of each other at a spacing of about 5-cm.

Heider et al. (1993) conducted a range of rock magnetic and electron microscope observations and concluded that the magnetostratigraphic signal of Eocene–Pliocene nannofossil oozes from the Kerguelen Plateau is carried by disseminated titanomagnetite particles originating from explosive volcanism on the Kerguelen archipelago. The AF demagnetization characteristics of the sediments analysed in this study (see below) are similar to those reported by Heider et al. (1993) for fine-grained titanomagnetites. We therefore do not include results of magnetic mineralogy investigations in this study.

4. Results

4.1. Hole 744A

Generally stable palaeomagnetic behaviour was observed in stepwise AF demagnetization data from Hole 744A. Examples of different types of observed demagnetization behaviour are shown in Fig. 2. In most cases, a weak secondary overprint is removed at low peak fields. ChRM directions generally tend toward the origin of the vector component diagrams (Fig. 2a,b); PCA was therefore constrained through the origin of the plots. Unusually, normal and reversed polarity overprints are both present in different parts of the core (Fig. 2c,d). Normal and reversed polarity overprints are sometimes observed in the same core sections (e.g. Hole 744A, core 20H, section 5). This provides evidence that the cores were not inadvertently inverted during initial handling on the ship or during u-channel sampling. These overprints were generally removed at peak fields of 35–40 mT and a clear ChRM component was still identified. The reversed polarity overprints are usually present in sediments that directly underlie thick stratigraphic intervals with reversed polarity (i.e. below 124.5–139 mbsf and 150–162 mbsf; Fig. 3). This suggests that the reversed polarity overprints might have resulted from delayed remanence acquisition in grains with the lowest coercivities. Mazaud (1996) suggested a model where a delayed remanence can be acquired up to several hundreds of thousands of years after deposition for a fraction of grains deposited when the palaeofield was weak. In this model, it is suggested that the field would not have been strong enough to efficiently align a proportion of the particles, which would then be aligned during a subsequent period of higher field intensity. In this case, the strength of the overprint would vary stratigraphically, which is the case in Hole 744A, and a reversed polarity overprint could be acquired in a reversed polarity field a few hundred kyr after deposition. Alternatively, if the particles have a long magnetic relaxation time, it is conceivable that they cumulatively acquired a 'hard' viscous remanent magnetization (VRM) through a series of reversals (Kok and Tauxe, 1996a,b). Rock magnetic evidence (Heider et al., 1993) suggests that part of the magnetic grain size assemblage in these sediments could be of an appropriate size for acquisition of a hard VRM. Thus, either a delayed remanence acquisition or cumulative VRM acquisition in part of the magnetic particle assemblage might explain the reversed polarity overprint and why an exclusively normal polarity VRM was not acquired during the Brunhes Chron. Finally, stable magnetizations were not evident for some intervals and no regular trend could be observed upon demagnetization (Fig. 2e). For such intervals, no palaeomagnetic interpretation was attempted. Relatively high coercivities were observed in some stratigraphic intervals (e.g. Fig. 2c). Heider et al. (1993) reported even higher coercivities than those shown in Fig. 2c for some samples, which they attributed to submicrometre titanomagnetite particles.

The dominance of demagnetization behaviour

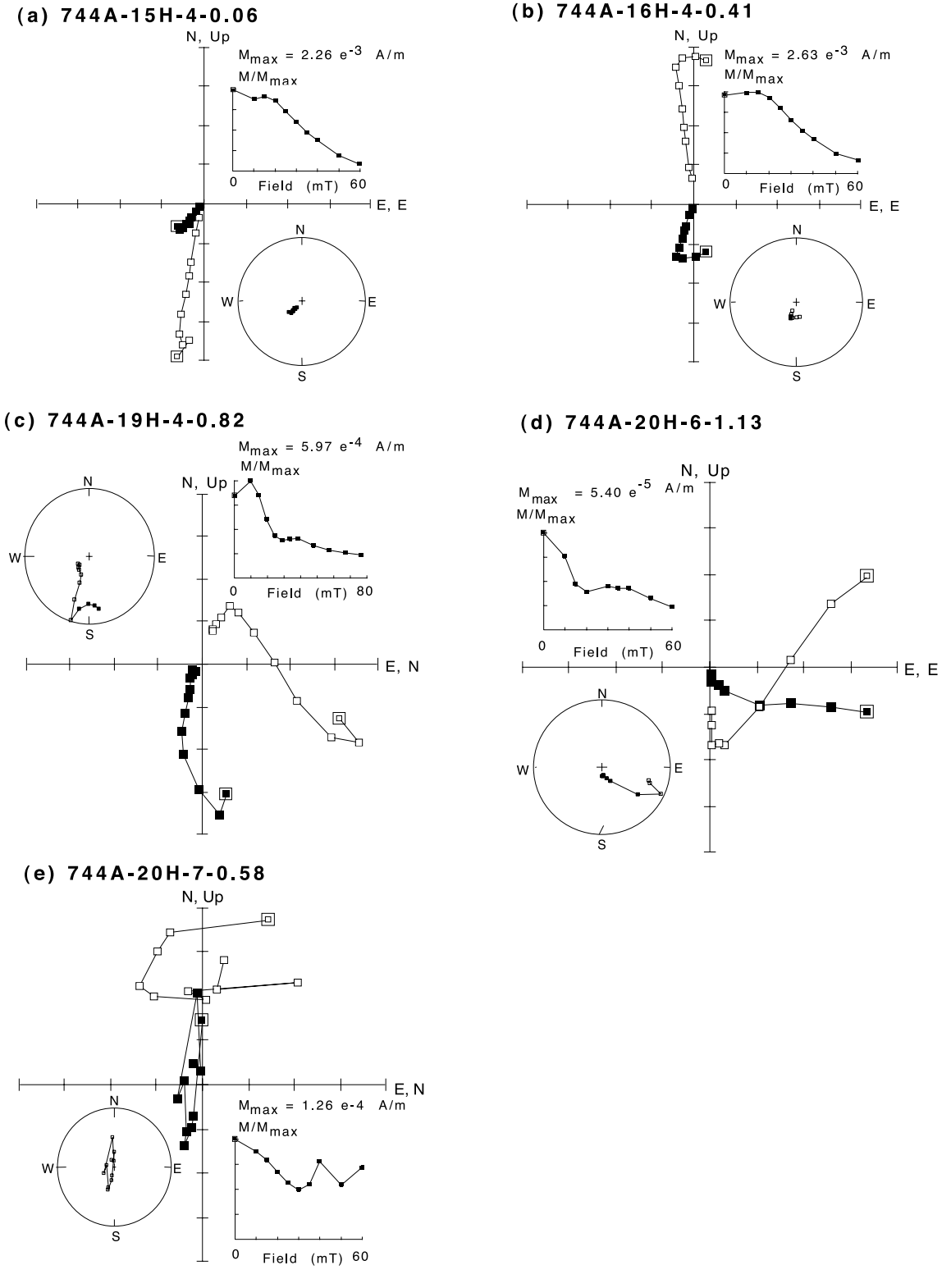
(a) 744A-15H-4-0.06
N, Up
M_{max} = 2.26 e^{-3} A/m
M/M_{max}
0 Field (mT) 60
E, E
N
W
E
S
(b) 744A-16H-4-0.41
N, Up
M_{max} = 2.63 e^{-3} A/m
M/M_{max}
0 Field (mT) 60
E, E
N
W
E
S
(c) 744A-19H-4-0.82
M_{max} = 5.97 e^{-4} A/m
M/M_{max}
N, Up
0 Field (mT) 80
E, N
N
W
E
S
(d) 744A-20H-6-1.13
N, Up
M_{max} = 5.40 e^{-5} A/m
M/M_{max}
0 Field (mT) 60
E, E
N
W
E
S
(e) 744A-20H-7-0.58
N, Up
E, N
M_{max} = 1.26 e-4 A/m
M/M_{max}
0 Field (mT) 60
N
W
E
S

like that shown in Fig. 2a,b allows construction of a magnetic polarity zonation for the studied interval of Hole 744A. The magnetic polarity data for the length of the studied interval are shown in Fig. 3, where palaeomagnetic inclinations are displayed alongside declinations and MAD values. The MAD values are generally $<4°$, which suggests that the data are of high quality. Higher MAD values were sometimes observed at polarity transitions and in intervals where the magnetization is relatively weak and where the palaeomagnetic signal is less easy to resolve. Within most polarity transitions, the magnetization is a composite of both polarities and transitional ChRM components were not clearly resolved. We therefore attempted no palaeomagnetic interpretation in most transitional intervals. Most transitions are only a few cm in thickness, so data gaps of the order of 5 cm are not evident in Fig. 3. Regardless, all MAD values are $<12°$, which is sufficiently precise to identify the polarity recorded by the sediment.

At the latitude of the site (61°34.66′S), the expected inclination for a geocentric axial dipole (GAD) field is $\pm 75°$. With such a steep expected inclination, the palaeomagnetic polarity can be uniquely determined from inclination data alone. The cores were not azimuthally oriented during coring. Thus, the palaeomagnetic declinations are only relative values. Declination values can also be affected by non-geomagnetic factors, such as core rotation during penetration of the core barrel into the sediment. Shifts in declination values are often evident at core breaks, even when the polarity remained constant. This is due to differences in orientation between the cores. Regardless, the declinations should change by 180° at each polarity reversal. Inspection of Fig. 3 indicates that this is the case for much of the studied interval and that the stable polarity intervals record the expected GAD inclination for the site latitude. Thus, it is clear that a stable and apparently reliable square-wave magnetostratigraphic signal can be discerned for the majority of the studied interval.

It should be noted that difficulties were encountered with recovery of core 17H and that only one section was recovered in this core (Barron et al., 1989). It appears that the palaeomagnetic data quality in the upper part of core 18H was also compromised by difficulties with coring (Fig. 3). This interval will be discussed further below. Also, the palaeomagnetic signal is not as clearly defined below 168 mbsf, where MAD values are generally higher and where declinations are more variable than in other studied intervals of Hole 744A.

4.2. Hole 748B

Stable palaeomagnetic behaviour was also generally observed in stepwise demagnetization data from Hole 748B. Examples of different types of observed demagnetization behaviour are shown in Fig. 4. The archive halves of the cores had been previously demagnetized at maximum peak AFs of 9 mT during shipboard analysis (Inokuchi and Heider, 1992). Application of such low fields means that analysis of the archive halves in this study was not compromised by the previous palaeomagnetic investigation. ChRM directions are generally easy to identify and tend toward the origin of the vector component diagrams (Fig. 4a,b); PCA was therefore constrained through the origin of the plots. Again, both normal and reversed polarity overprints are present in different parts of the core (Fig. 4c–e); however, these overprints are stronger than in Hole 744A and can persist to much higher applied fields (Fig. 4d,e). Within portions of the core, it is clear

Fig. 2. Vector component diagrams illustrating the range of AF demagnetization results observed for the studied interval of Hole 744A. Open (closed) symbols represent projections onto the vertical (horizontal) plane. The stereoplots are equal-area stereographic projections, where solid (open) symbols represent lower (upper) hemisphere projections. Examples of sediments with: (a) stable reversed polarity (132.18 mbsf); (b) stable normal polarity (142.11 mbsf); (c) normal polarity with a low-coercivity reversed polarity overprint (162.42 mbsf); (d) reversed polarity with low-coercivity normal polarity overprint (174.64 mbsf); and (e) unstable magnetization (175.59 mbsf). Note: the cores are not azimuthally oriented, so the declinations do not represent expected geomagnetic values.

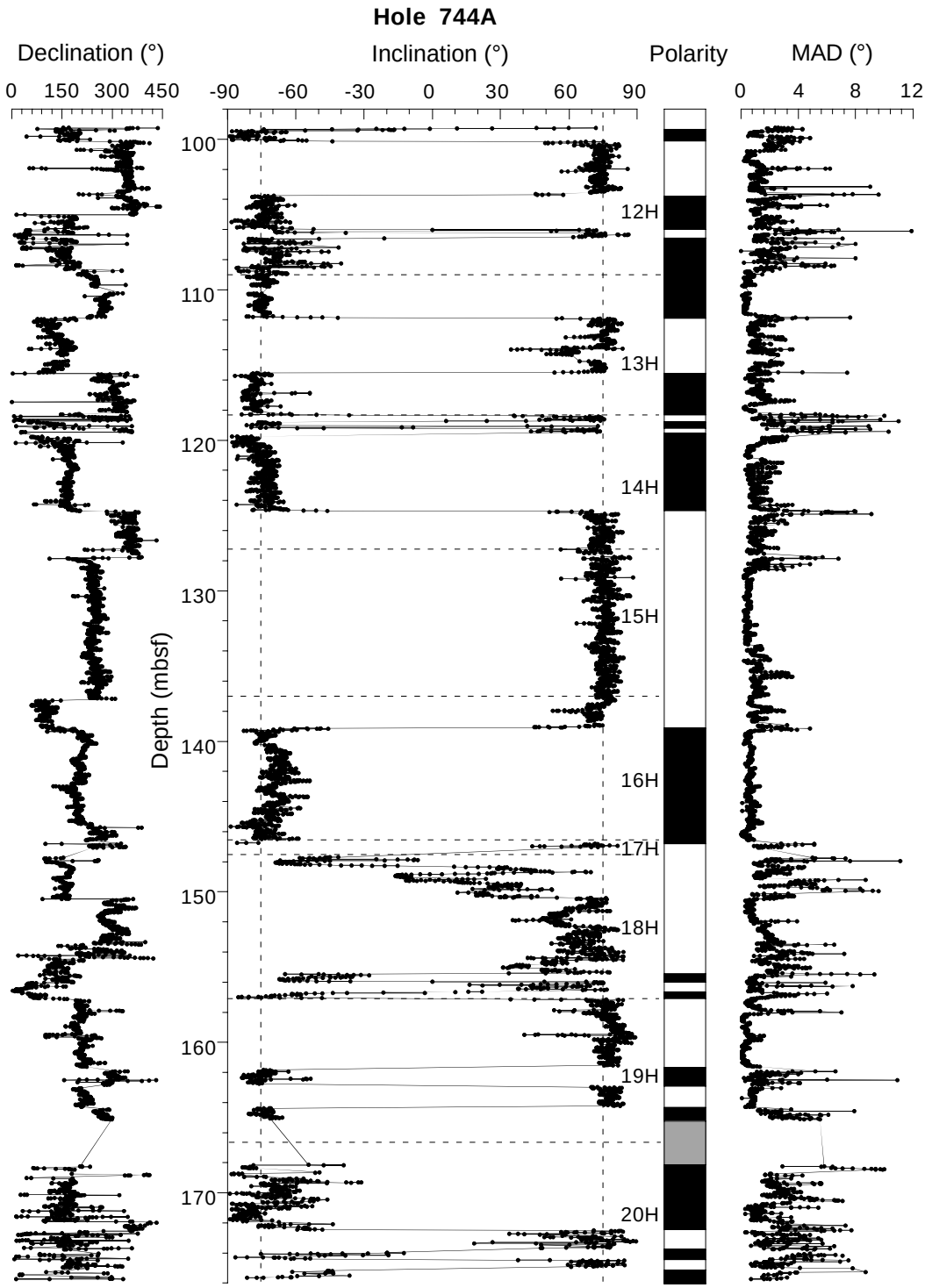

Fig. 3. Palaeomagnetic declinations, inclinations and MAD values for ChRM directions, plotted at 1-cm stratigraphic intervals, for Hole 744A. Some of the declinations are arbitrarily shown as D+360° for the sake of clarity. Dashed vertical lines indicate the inclinations expected for a GAD field at the site latitude. Dashed horizontal lines indicate core breaks. Black (white) indicates normal (reversed) polarity.

that the strength of the overprint varies with stratigraphic position, and, in places, it almost obliterates the remaining ChRM. In such cases, examination of the demagnetization behaviour across a stratigraphic interval makes it clear that the magnetization is dominated by an overprint and no interpretation was made when the overprint dominates the NRM. Our hypothesized explanation of the mechanism for the observed strong reversed polarity overprints is the same as for Hole 744A. Stable magnetizations were not evident in some cases, particularly below 122.51 mbsf, and no regular trend was observed upon demagnetization (Fig. 4f). For such intervals, no palaeomagnetic interpretation was attempted.

As was the case for Hole 744A, the dominance of demagnetization behaviour like that shown in Fig. 4a,b means that it is straightforward to construct a magnetic polarity zonation for the studied interval of Hole 748B (Fig. 5). Again, MAD values are generally $<4°$ and always $<12°$. Relatively high MAD values are often observed at polarity transitions and in intervals where the magnetization is relatively weak. In particular, the palaeomagnetic behaviour is not as consistently stable between 114 and 122.51 mbsf and this is reflected in the higher MAD values. Within the Eocene, below 122.51 mbsf, the magnetizations are weaker and much less stable than for the Oligocene sediments. We therefore do not present results below this depth.

The expected inclination for a GAD field is $\pm 73°$ at the latitude of the site (58°26.45′S). The steep palaeomagnetic inclinations provide a clear indication of the polarity, and, as expected, declination shifts of 180° are evident at most of the polarity reversals (Fig. 5). Overall, the clear square-wave palaeomagnetic signal, with bimodal distribution of inclinations coinciding with the value expected for a GAD field at the latitude of the respective sites (Fig. 6), suggests that the magnetic polarity signal is robust for holes 744A and 748B. Additionally, careful inspection of vector component diagrams (Figs. 2 and 4) indicates that secondary overprints have been adequately removed for sediments from both holes.

5. Discussion

5.1. Hole 744A

The stability of the magnetic signal in the Eocene–Oligocene portion of Hole 744A (Fig. 2), with secondary magnetic overprints being removed at relatively low fields, suggests that the blanket demagnetization treatment of Keating and Sakai (1991) enabled identification of the correct palaeomagnetic polarity. Thus, our results generally verify those of Keating and Sakai (1991). However, because of the low sampling density of the previous study, we identify a few more short polarity intervals in our high-resolution study compared to Keating and Sakai (1991). For example, there are minor discrepancies between the two data sets in the intervals around 106, 119, 155–158, and between 165 and 170 mbsf. In addition, our study enables more precise identification of the boundaries of polarity intervals in Hole 744A.

In the following discussion, we provide an interpretation of the magnetic polarity pattern using the biostratigraphic data of Wei and Thierstein (1991) and Huber (1991), which enables development of a revised calibration of the diatom biostratigraphy of Baldauf and Barron (1991) for Hole 744A. It should be noted that the Eocene–Oligocene diatom age calibrations for the Southern Ocean are primarily based on published data from holes 744A and 748B. We have therefore been careful to avoid circular reasoning by checking our interpretations with calibrations of calcareous nannofossil and planktonic foraminiferal datums and then applying revised ages based on this cross-calibration to the diatom datums.

Our magnetostratigraphic interpretation for Hole 744A is presented in Fig. 7 and is based on correlation with the geomagnetic polarity timescale (GPTS) of Cande and Kent (1992, 1995). The positions of biostratigraphic datums are shown along with the stratigraphic uncertainties associated with each datum (see Table 1 for details). $^{87}Sr/^{86}Sr$ ages are also shown in Fig. 7 along with their respective age uncertainties (Table 2). We recalculated the $^{87}Sr/^{86}Sr$ ages from the Sr values of Barrera et al. (1991), using the marine

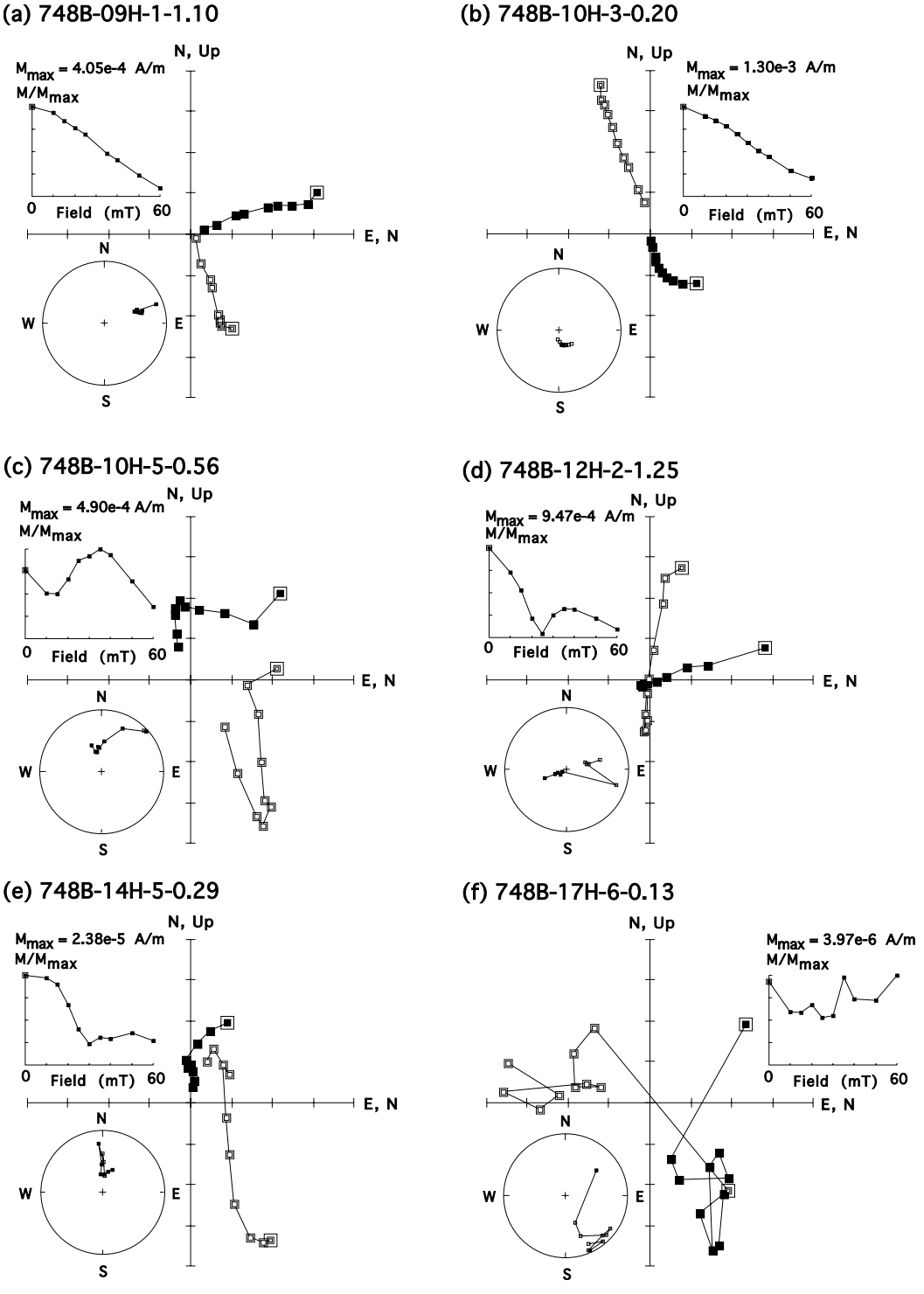
(a) 748B-09H-1-1.10
N, Up
M_{max} = 4.05e-4 A/m
M/M_{max}
0 Field (mT) 60
E, N
N
W
E
S
(b) 748B-10H-3-0.20
N, Up
M_{max} = 1.30e-3 A/m
M/M_{max}
0 Field (mT) 60
E, N
N
W
E
S
(c) 748B-10H-5-0.56
N, Up
M_{max} = 4.90e-4 A/m
M/M_{max}
0 Field (mT) 60
E, N
N
W
E
S
(d) 748B-12H-2-1.25
N, Up
M_{max} = 9.47e-4 A/m
M/M_{max}
0 Field (mT) 60
E, N
N
W
E
S
(e) 748B-14H-5-0.29
N, Up
M_{max} = 2.38e-5 A/m
M/M_{max}
0 Field (mT) 60
E, N
N
W
E
S
(f) 748B-17H-6-0.13
N, Up
M_{max} = 3.97e-6 A/m
M/M_{max}
0 Field (mT) 60
E, N
N
W
E
S

Sr-isotope curve of McArthur et al. (2001), which is tied to the GPTS of Cande and Kent (1995).

The upper Eocene–upper Oligocene interval (~100–175 mbsf) appears to contain two disconformities in Hole 744A and correlation to the GPTS is achieved using all available chronostratigraphic constraints (Fig. 7). The 14-m thick interval of reversed polarity between 125 and 139 mbsf can be correlated with Chron C12r, which is the longest interval of reversed polarity (2 Myr) in the late Palaeogene. Correlation of the palaeomagnetic polarity pattern in Hole 744A with the GPTS above and below Chron C12r provides a reasonable age interpretation between chrons C12n and C16r (30.5–36.5 Ma). The only mismatches with the GPTS in this interval are the normal polarity zone in C13r at 148 mbsf (Fig. 3) and the reversed polarity zones in C15n and C17n at 156 and 174.5 mbsf (Fig. 7), respectively. The thin normal polarity zone at 148 mbsf corresponds to an interval of disturbed core within the upper part of core 18H (Barron et al., 1989), which we do not consider to represent real geomagnetic field behaviour. The reversed polarity data at 156 mbsf appear to be robust and are therefore anomalous in terms of providing a straightforward match with the GPTS. It should be noted, however, that Keating and Sakai (1991) recognised two thin reversed polarity zones in this interval of Hole 744A. Thus, our results for this interval are less anomalous than those of Keating and Sakai (1991). The reversed polarity data at 174.5 mbsf occur within an interval with multiple remanence components; however, these data appear to be robust. Despite the presence of two thin anomalous reversed polarity zones at 156 and 174.5 mbsf, the palaeomagnetic polarity pattern seems to clearly match the GPTS. Independent verification of this age interpretation is provided by calcareous nannofossil datums and $^{87}Sr/^{86}Sr$ ages. Previously calibrated ages (Berggren et al., 1995) for the last occurrence (LO) of *Reticulofenestra umbilica* (N3), the LO of *R. oamaruensis* (N4), and the first occurrence (FO) of *Isthmolithus recurvus* (N6) (Table 1) fall precisely on, or close to, our interpreted correlation line. The $^{87}Sr/^{86}Sr$ ages recalculated from Barrera et al. (1991) also fall on, or close to, the correlation line. However, the ages for the LO of *Globigerapsis index* (P6) and the FO of *R. oamaruensis* (N5) are slightly younger than interpreted here. Also, the peak of the Oi-1 $\delta^{18}O$ event occurs at 146.11 mbsf in Hole 744A (Zachos et al., 1996) and at 115.09 in Hole 748B (Zachos et al., 1992), which is at the base of Chron C13n in both holes. Thus, our age interpretation for the upper Eocene–lower Oligocene interval of Hole 744A is consistent with most available additional constraints. It should be noted that Zachos et al. (1999) reported a coincidence between subtle steps in $^{87}Sr/^{86}Sr$ ratios and climatically driven $\delta^{18}O$ variations for the studied interval of Hole 748B. They suggested that there was a climatic influence on continental weathering that affected the seawater Sr values. These short-term Sr variations are not represented in the averaged Sr seawater curve of McArthur et al. (2001), which might explain why some of the $^{87}Sr/^{86}Sr$ dates do not fall precisely on the age–depth correlation lines presented for holes 744A and 748B (Figs. 7 and 8).

Interpretation of the late Oligocene portion of Hole 744A is more difficult compared to the late Eocene–early Oligocene portion and several interpretations are possible. A sedimentary hiatus, with duration of up to 2.5 Myr, is evident at ~117–119 mbsf (Fig. 7). The exact position of the hiatus is uncertain, as indicated in Fig. 7. The presence and position of the hiatus are constrained by the coincident LO of *Chiloguembelina cubensis* (P4) and *Subbotina angiporoides* (P5). This hiatus is also identified on the basis of Sr-isotope stratigraphy (Barrera et al., 1991). It is

Fig. 4. Vector component diagrams illustrating the range of AF demagnetization results observed for the studied interval of Hole 748B. The conventions are the same as in Fig. 2. Examples of sediments with: (a) stable reversed polarity (67.70 mbsf); (b) stable normal polarity (79.3 mbsf); (c) reversed polarity with a low-coercivity normal polarity overprint (82.66 mbsf); (d) reversed polarity with a slightly higher-coercivity normal polarity overprint (97.4 mbsf); (e) normal polarity with a reversed polarity overprint (120.09 mbsf); and (f) unstable magnetization (142.6 mbsf). Note: the cores are not azimuthally oriented, so the declinations do not represent expected geomagnetic values.

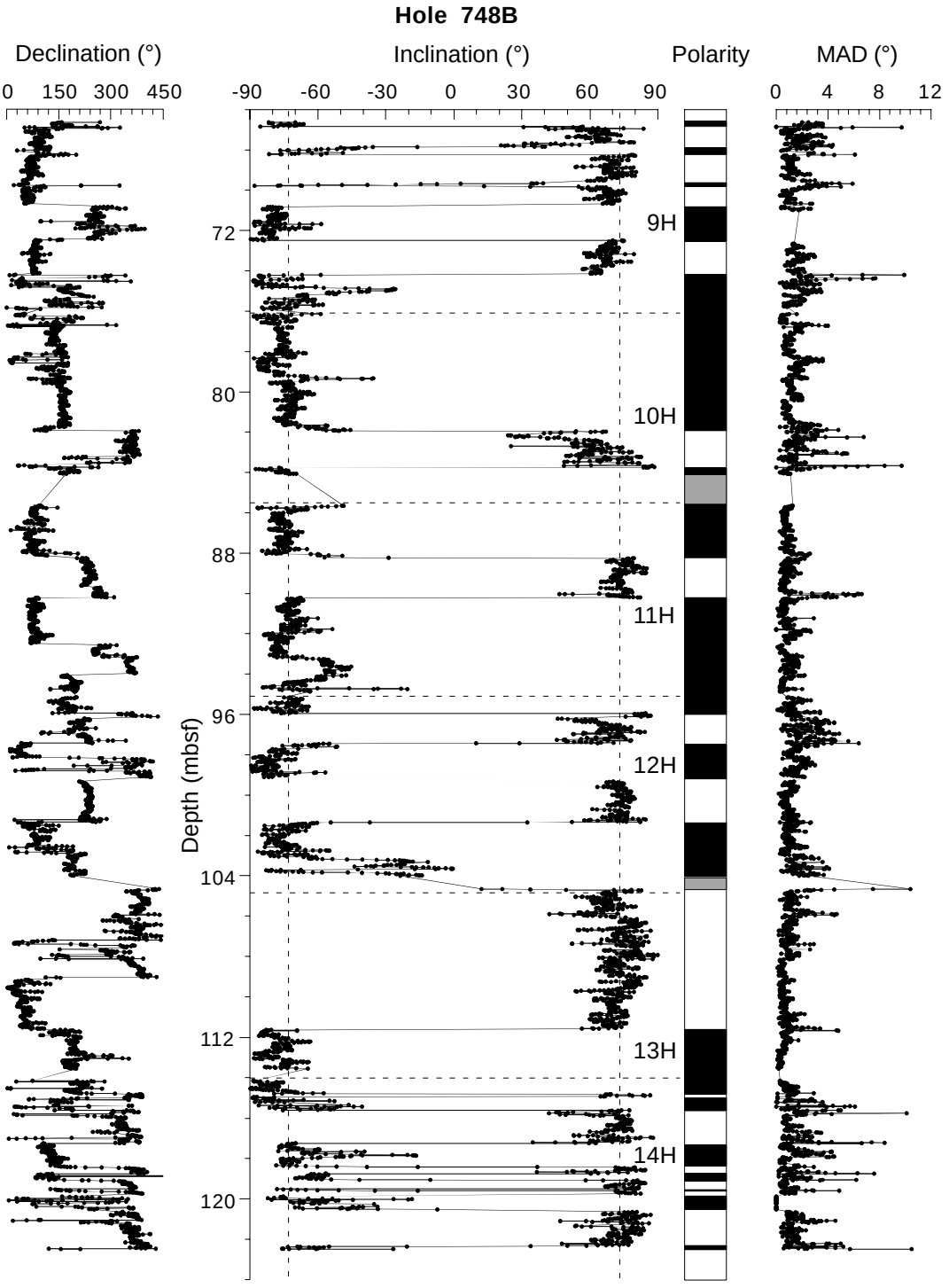

Fig. 5. Palaeomagnetic declinations, inclinations and MAD values for ChRM directions, plotted at 1-cm stratigraphic intervals, for Hole 748B. Some of the declinations are arbitrarily shown as D+360° for the sake of clarity. Dashed vertical lines indicate the inclinations expected for a GAD field at the site latitude. Dashed horizontal lines indicate core breaks. Black (white) indicates normal (reversed) polarity.

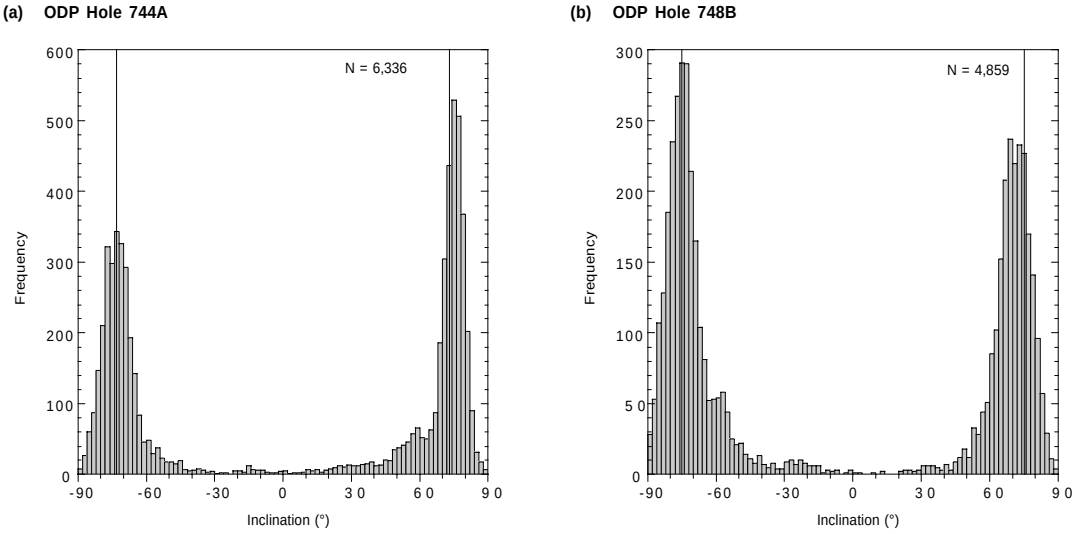

Fig. 6. Histogram of ChRM inclinations shown in Figs. 3 and 5 for (a) Hole 744A and (b) Hole 748B, respectively. The expected inclinations for a GAD field at the respective site latitudes are also shown. The statistical mode for normal and reversed polarity data for both holes is coincident with the expected GAD values, which provides evidence that the data sets are robust.

difficult to interpret the magnetic polarity pattern in the immediate vicinity of this unconformity. Based on the LO of *C. cubensis* (P4), the relative thicknesses of polarity zones above this level and inferred average sedimentation rates, the polarity zones between 106.5 and 118 mbsf correlate reasonably well with chrons C9n to C10n.1n. With this interpretation, there is a slight discrepancy with the position of the LO of *Globigerina labiacrassata* (P3) and the LO of *Chiasmolithus altus* (N2), although P3 occurs in the same subchron as calibrated by Berggren et al. (1995). This interpretation also only just fits with the oldest ages permitted by the $^{87}Sr/^{86}Sr$ ages converted from Barrera et al. (1991).

In the uppermost Oligocene, based on the absence of the *Rocella gelida* 'b' Subzone of Harwood and Maruyama (1992), there appears to be an unconformity at ~105–106 mbsf in Hole 744A, where the ranges of *R. vigilans* and *Lisitzinia ornata* are truncated. This interpretation is supported by the presence of a manganese nodule in core 12H-4–135 cm (see lithological logs in Barron et al., 1989). Mn nodules form during prolonged exposure at the sea floor, which suggests that the hiatus occurred at 105.05 mbsf. Datums N1 (LO *Dictyococcites bisectus*) and P1 (LO *Globigerina euapertura*) suggest that the normal polarity interval at the top of the section is likely to represent Chron C6Cn.3n and the underlying 4-m thick zone of reversed polarity is most likely to represent Chron C6Cr. While this interpretation fits the biostratigraphic and magnetostratigraphic constraints, it is difficult to reconcile with the strontium isotope age (S2) at 101.67 mbsf (Fig. 7).

Three additional notes are worth making about the interpretation presented here for Hole 744A. First, although preservation of siliceous microfossils is moderate to poor in this part of holes 744A and 748B, Baldauf and Barron (1991) reported the FO of *Cavitatus jouseanus* (D8) between 123.31 and 124.81 mbsf in Hole 744A. This places the datum in the basal part of Chron C12n, which is consistent with our interpretations for Hole 748B (Table 3). Ramsay and Baldauf (1999) mistakenly listed the FO of *C. jouseanus* in Hole 744A at between 118.82 and 120.32 mbsf, which wrongly places the datum at a major unconformity (Fig. 7). It should be noted that the *Cavitatus* lineages in holes 744A and 748B need more thorough investigation, particularly concerning the FO of early forms of *C. jouseanus*. Second, there were slight differences in the diatom taxonomy

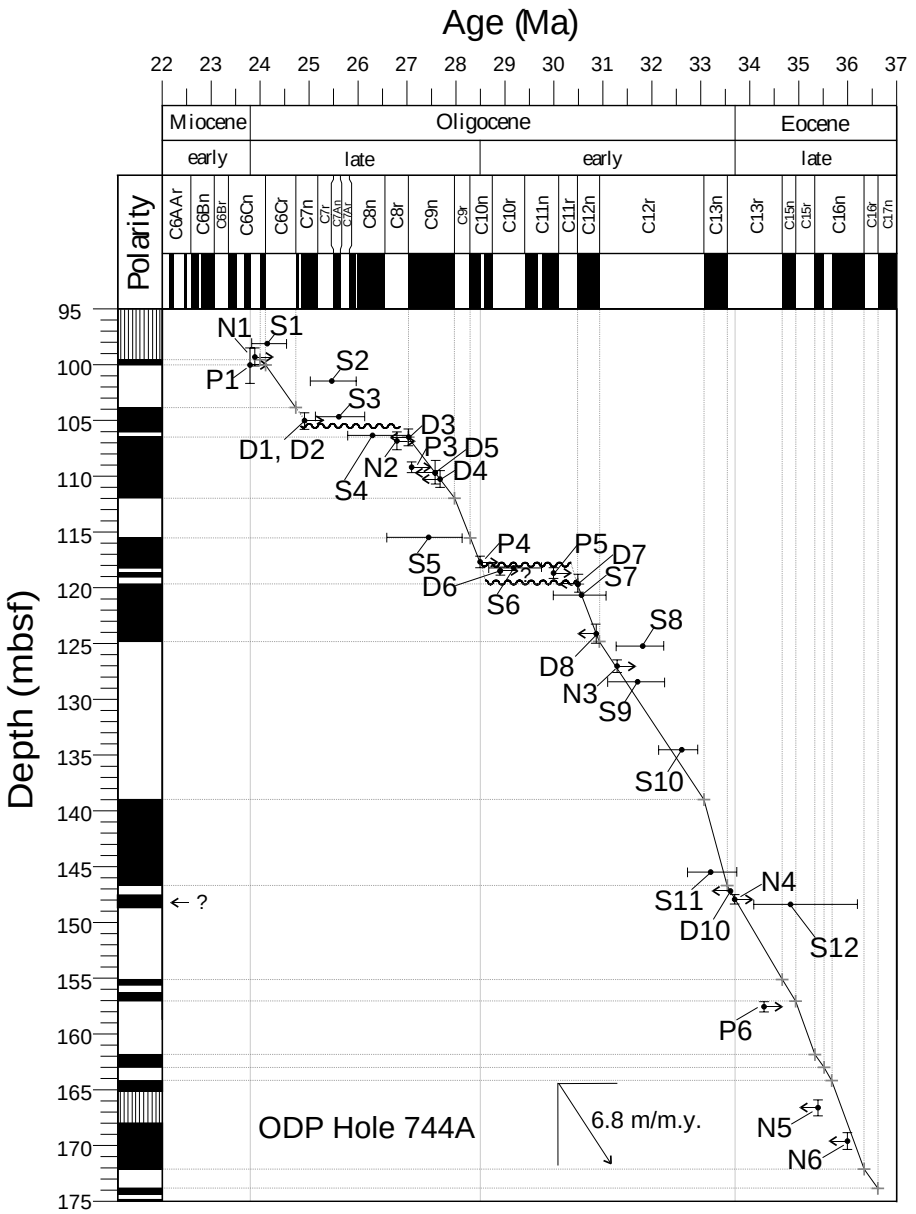

Fig. 7. Age versus depth plot with correlation of the Hole 744A polarity zonation to the GPTS of Cande and Kent (1995). Calcareous nannofossil (N) and planktonic foraminiferal (P) datums (from Berggren et al., 1995; Table 1) and $^{87}Sr/^{86}Sr$ (S) ages (from Barrera et al., 1991; Table 2) are used to constrain the interpretations. Diatom datums (D) are calibrated in this study and are shown on the correlation line at the depths where they occur in Hole 744A (Table 1). Age calibrations of the diatom datums are listed in Table 3. The question mark beside the thin normal polarity interval at ~148 mbsf indicates uncertainty due to coring disturbances. The question mark between 118 and 120 mbsf indicates uncertainty concerning the position of the inferred unconformity.

Table 1
Biostratigraphic datums from Eocene–Oligocene sediments in ODP holes 744A and 748B

	Hole 744A upper sample	Upper depth interval (mbsf)	Hole 744A lower sample	Lower depth interval (mbsf)	Average depth (mbsf)	± m	Hole 748B upper sample	Upper depth interval (mbsf)	Hole 748B lower sample	Lower depth interval (mbsf)	Average depth (mbsf)	± m	Age	Calibration	Designation
Calcareous nannofossils															
LO *Dictyococcites bisectus*[a]	11H-CC	98.50	12H-1, 92–93	100.12	99.31	0.81	8H-7, 55–59	66.65	9H-1, 10–11	66.70	66.68	0.03	23.9	BK95	N1
LO *Chiasmolithus altus*	12H-5, 92–93	106.12	12H-6, 92–93	107.62	106.87	0.75	9H-5, 10–11	72.70	9H-6, 10–11	74.20	73.45	0.75	26.8	BK95[b]	N2
LO *Reticulofenestra umbilica*	14H-6, 75–76	126.45	14H-CC	127.60	127.03	0.57	12H-7, 10–11	104.20	13H-1, 10–11	104.70	104.45	0.25	31.3	BK95	N3
LO *Isthmolithus recurvus*	15H-2, 75–76	129.95	15H-3, 75–76	131.45	130.70	0.75	13H-4, 10–11	109.20	13H-5, 10–11	110.70	109.95	0.75			
LO *Reticulofenestra oamaruensis*	17H-CC	147.50	18H-1, 75–76	148.35	147.93	0.42	14H-2, 24–26	115.84	14H-2, 35–39	115.95	115.90	0.06	33.7	BK95	N4
FO *Reticulofenestra oamaruensis*	19H-CC	166.15	20H-1, 75–76	167.35	166.75	0.60	15H-2, 10–11	125.20	15H-3, 10–11	126.70	125.95	0.75	35.4	BK95	N5
FO *Isthmolithus recurvus*	20H-2, 75–76	168.85	20H-3, 75–76	170.35	169.60	0.75	15H-3, 10–11	126.70	15H-4, 10–11	128.20	127.45	0.75	36.0	BK95	N6
LO *Cribrocentrum reticulatum*[c]	–	–	–	–	–	–	15H-4, 10–11	128.20	15H-5, 10–11	129.70	128.95	0.75	36.1	BK95	N7
FO *Chiasmolithus oamaruensis*	–	–	–	–	–	–	17H-3, 10–11	145.70	17H-4, 10–11	147.20	146.45	0.75	37.0	BK95	
LO *Chiasmolithus solitus*	–	–	–	–	–	–	17H-5, 10–11	148.70	17H-6, 10–11	150.20	149.45	0.75	40.4	BK95	
FO *Cribrocentrum reticulatum*[c]	–	–	–	–	–	–	19H-7, 10–11	170.70	20H-1, 10–11	171.20	170.95	0.25	42.0	BK95	
FO *Reticulofenestra umbilica*	–	–	–	–	–	–	–	–	–	–	–	–			
Planktonic foraminifera															
LO *Globigerina euapertura*	11H-CC	98.50	12H-2, 96–101	101.68	100.09	1.59	8H-5, 40–44	63.50	8H-6, 40–44	65.00	64.25	0.75	23.8	BK95	P1
LO *Tenuitella gemma*	–	–	–	–	–	–	9H-1, 40–44	67.00	9H-2, 40–44	68.50	67.75	0.75	24.3	BK95	P2
LO *Globigerina labiacrassata*	12H-CC	108.70	13H-1, 95–100	109.67	109.19	0.48	10H-4, 40–44	81.00	10H-5, 40–44	82.50	81.75	0.75	27.1	BK95	P3
LO *Chiloguembelina cubensis*	13H-6, 95–100	117.17	13H-CC	118.20	117.69	0.52	10H-6, 34–38	83.90	10H-CC	85.60	84.75	0.85	28.5	BK95	P4
LO *Subbotina angiporoides*	13H-CC	118.20	14H-1, 95–100	119.17	118.69	0.48	12H-2, 80–84	97.40	12H-3, 40–44	98.50	97.95	0.55	30.0	BK95	P5
LO *Globigerapsis index*	18H-CC	157.10	19H-1, 90–95	158.02	157.56	0.46	14H-5, 40–44	120.50	14H-6, 80–84	122.40	121.45	0.95	34.3	BK95	P6
LO *Acarinina collactea*	–	–	–	–	–	–	16H-6, 40–44	140.83	16H-7, 80–84	141.95	141.39	0.56	37.7	BK95	
LCO *Subbotina linaperta*	–	–	–	–	–	–	17H-1, 80–84	143.40	17H-2, 80–84	144.90	144.15	0.75	37.7	BK95	
LO *Acarinina primitiva*	–	–	–	–	–	–	18H-1, 40–44	152.50	18H-2, 80–84	154.40	153.45	0.95	39.0	BK95	
Diatoms															
FO *Thalassiosira praefraga*	11H-1, 63–65	90.34	11H-2, 63–65	91.84	91.09	0.75	8H-2, 47–49	59.08	8H-3, 47–49	60.58	59.83	0.75			
LO *Rocella gelida*[d]	11H-4, 63–65	94.84	11H-5, 63–65	96.34	95.59	0.75	7H-6, 47–48	55.67	7H-CC	56.95	56.31	0.64			
LO *Lisitzinia ornata*[d]	12H-4, 60–62	104.31	12H-5, 60–62	105.81	105.06	0.75	9H-2, 100–102	69.11	9H-3, 47–49	70.08	69.60	0.48			D1
LO *Rocella vigilans* var. B[d]	12H-4, 60–62	104.31	12H-5, 60–62	105.81	105.06	0.75	9H-3, 100–102	70.61	9H-4, 47–49	71.58	71.10	0.48			D2
FO *Rocella gelida*[d,e]	12H-5, 60–62	105.81	12H-6, 60–62	107.31	106.56	0.75	9H-3, 100–102	70.61	9H-4, 47–49	71.58	71.10	0.48			D3
FO *Lisitzinia ornata*	13H-1, 60–62	109.31	13H-2, 60–62	110.81	110.06	0.75	10H-3, 47–49	79.58	10H-4, 47–49	81.08	80.33	0.75			D4
FO *Rocella vigilans* var. B[e]	12H-CC	108.70	13H-2, 60–62	110.81	109.76	1.06	10H-3, 47–49	79.58	10H-4, 47–49	81.08	80.33	0.75			D5
LCO *Rocella vigilans* var. A[e]	13H-CC	118.15	14H-1, 64–66	118.85	118.50	0.35	11H-3, 47–49	89.08	11H-4, 47–49	90.58	89.83	0.75			D6
FO *Rocella vigilans* var. A[d,e]	14H-1, 64–66	118.85	14H-2, 60–62	120.31	119.58	0.73	12H-3, 47–49	98.58	12H-3, 100–102	99.11	98.85	0.27			D7
FO *Cavitatus jouseanus*[f]	14H-4, 60–62	123.31	14H-5, 60–62	124.81	124.06	0.75	12H-6, 47–49	103.08	12H-7, 47–49	104.58	103.83	0.75			D8
FO *Rhizosolenia antarctica*	–	–	–	–	–	–	13H-5, 116–118	111.77	13H-6, 116–118	113.27	112.52	0.75			D9
FO *Rhizosolenia oligocaenica*[e]	16H-CC	147.20	17H-CC	147.50	147.35	0.15	14H-1, 52–54	114.63	14H-4, 47–49	119.08	116.86	2.22			D10

Nannofossil data are from Wei and Thierstein (1991), Wei and Wise (1992), and Wei et al. (1992); planktonic foraminifera data are from Huber (1991) and Berggren (1992); diatom data are from Baldauf and Barron (1991) and Harwood and Maruyama (1992). Revised ages for biostratigraphic datums with respect to the geomagnetic polarity timescale are reported in Berggren et al. (1995) = BK95.

[a] Syn. *Reticulofenestra bisecta*.
[b] Calibration at Site 522 from references in BK95.
[c] Syn. *Reticulofenestra reticulata*.
[d] Position of diatom datum in Hole 748B has been modified in this study as a result of reexamination of samples.
[e] Position of diatom datum in Hole 744A has been modified in this study as a result of either taxonomic considerations or reexamination of samples.
[f] Syn. *Synedra jouseana*.

Table 2
Sr-isotope ages for Eocene–Oligocene sediments from ODP holes 744A and 748B

Core, section, interval (cm)	Depth (mbsf)	$^{87}Sr/^{86}Sr$[a]	$^{87}Sr/^{86}Sr$[b]	2σ[a]	Age (Ma)	Minimum age (Ma)	Maximum age (Ma)	Designation
ODP Hole 744A								
11H-6, 100–105	98.13	0.708242	0.708245	16	24.20	23.80	24.57	S1
12H-2, 96–101	101.67	0.708163	0.708166	16	25.47	25.01	25.98	S2
12H-4, 95–100	104.67	0.708156	0.708159	16	25.61	25.13	26.14	S3
12H-5, 95–100	106.17	0.708121	0.708124	17	26.34	25.78	27.03	S4
13H-5, 95–100	115.67	0.708082	0.708085	18	27.41	26.59	28.13	S5
13H-CC	118.20	0.708013	0.708016	13	29.19	28.63	29.74	S6
14H-2, 95–100	120.67	0.707960	0.707963	11	30.54	30.00	31.09	S7
14H-5, 95–100	125.17	0.707911	0.707914	11	31.78	31.31	32.23	S8
15H-1, 95–100	128.67	0.707916	0.707919	17	31.67	31.04	32.25	S9
15H-5, 95–100	134.67	0.707873	0.707876	14	32.57	32.11	32.95	S10
16H-6, 95–100	145.67	0.707838	0.707841	18	33.21	32.71	33.75	S11
18H-1, 95–100	148.57	0.707778	0.707781	13	34.84	34.07	36.24 (49.15)	S12
ODP Hole 748B								
9H-1-40–44	67.00	0.708190	0.708194	14	24.97	24.64	25.38	S1
11H-2-40–44	87.50	0.708010	0.708014	14	29.24	28.65	29.82	S2
12H-3-100–102	99.10	0.707953	0.707957	14	30.71	30.08	31.33	S3
12H-7-40–44	104.50	0.707950	0.707954	14	30.79	30.16	31.40	S4
13H-2-18–22	106.28	0.707882	0.707886	14	32.39	31.89	32.78	S5
13H-4-80–84	109.90	0.707890	0.707894	16	32.22	31.67	32.68	S6
13H-6-18–22	112.28	0.707824	0.707828	17	33.47	32.95	33.97	S7
14H-1-80–84	114.90	0.707830	0.707834	14	33.35	32.90	33.82	S8
14H-2-138–142	116.98	0.707796	0.707800	14	34.13	33.97	35.04 (46.10)	S9
14H-3-138–142	118.48	0.707763	0.707767	14	35.70	34.46	37.63 (50.25)	S10
14H-4-138–142	119.98	0.707808	0.707812	16	33.81	33.30	34.53	S11
14H-5-40–44	120.50	0.707757	0.707761	14	36.13	34.72	38.33 (50.68)	S12
14H-5-97–101	121.11	0.707788	0.707792	14	34.38	33.76	35.50 (48.22)	S13
14H-5-97–101	121.11	0.707766	0.707770	14	35.47	34.37	37.33 (50.04)	S14
14H-5-138–142	121.48	0.707771	0.707775	14	35.18	34.21	36.90 (49.68)	S15
14H-6-138–142	121.48	0.707775	0.707779	14	34.96	34.10	36.51 (49.38)	S16
14H-6-138–142	122.98	0.707774	0.707778	14	35.02	34.12	36.60 (49.45)	S17

Ages were determined for the $^{87}Sr/^{86}Sr$ values using the look-up tables of McArthur et al. (2001). Minimum and maximum ages were determined using the 2σ uncertainties and the look-up tables. Numbers in parentheses indicate maximum ages where the slope of the Sr curve is flat and less useful for determining maximum ages.

[a] Original $^{87}Sr/^{86}Sr$ ratios and 2σ values for Hole 744A are from Barrera et al. (1991) and from Zachos et al. (1999) for Hole 748B. The $^{87}Sr/^{86}Sr$ data are from planktonic foraminifera only.

[b] The $^{87}Sr/^{86}Sr$ ratios were normalized to NIST-987 = 0.710248 (McArthur et al., 2001) by adjusting the values for Hole 744A by adding 3×10^{-6} and the values for Hole 748B by adding 4×10^{-6}. The 2σ values of Zachos et al. (1999) were adjusted to a minimum of 14 to reflect the maximum precision for multiple runs of the NIST-987 Sr standard.

originally applied to holes 748B and 744A. The LO of '*R. vigilans* var. B' (D2) of Harwood and Maruyama (1992) is equivalent to the LO of '*R. vigilans*' of Baldauf and Barron (1991). Also, the FO of *R. gelida* in Hole 744A (Baldauf and Barron, 1991) is actually the FO of *R. vigilans* var. B. Third, Keating and Sakai (1991) acknowledged that their sampling resolution was insufficient to document all of the polarity intervals that should be recorded in Hole 744A. The frequency of geomagnetic reversals was lower in the Eocene–Oligocene than in the Miocene (Cande and Kent, 1992, 1995), so the sampling problem is more likely to be severe in the Miocene, where high-resolution magnetostratigraphic results are not available. It would therefore be prudent to treat the Neogene magnetostratigraphic interpretation of Keating and Sakai (1991) with care and future high-resolution palaeomagnetic work on this part of Hole 744A is warranted.

5.2. Hole 748B

The presence of strong secondary magnetization components in Hole 748B, which sometimes almost completely obscure the ChRM, makes this record more difficult to interpret (in places) than that from Hole 744A. These overprints were not recognised by Inokuchi and Heider (1992), who only demagnetized the cores on a routine basis to maximum peak fields of 9 mT. Recognition of these overprints in the present study means that the polarity zonation shown in Fig. 5 differs substantially from that of Inokuchi and Heider (1992). The following discussion therefore involves a complete re-interpretation of the polarity record from Hole 748B. In addition, the $^{87}Sr/^{86}Sr$ ratios published by Zachos et al. (1999) have been converted to ages using the look-up tables of McArthur et al. (2001) and are used to constrain the chronostratigraphic interpretation.

The discrepancies between our study and that of Inokuchi and Heider (1992) illustrate one of the advantages of the u-channel approach to magnetostratigraphic studies. The level of resolution afforded by this method enables much closer scrutiny of stratigraphic variations in demagnetization behaviour. Careful inspection of demagnetization diagrams at 1-cm intervals provides a higher likelihood of identifying zones where interpretation might be difficult. While strong coring-induced magnetic overprints are commonly observed in ODP cores (e.g. Stokking et al., 1993; Roberts et al., 1996; Fuller et al., 1998), the overprints usually have exclusively either normal or reversed polarity. In our extensive palaeomagnetic experience of ODP cores (eight legs), we have never observed both normal and reversed polarity overprints in the same hole. Thus, we attribute the presence of these overprints to the rock magnetic characteristics of the Kerguelen Plateau sediments, which, based on the results of Heider et al. (1993), contain the necessary fine single-domain particles for acquisition of secondary magnetizations in the models of Mazaud (1996) or Kok and Tauxe (1996a,b). Specifically, the long intervals of reversed polarity in the late Eocene and Oligocene (up to 2 Myr in duration) might contribute to these unusual reversed polarity overprints through either proposed mechanism.

As is the case for Hole 744A, the easiest place to begin our interpretation of the Hole 748B magnetostratigraphy is in the early Oligocene, where Chron C12r represents 2 Myr of reversed polarity. We correlate the thickest interval of reversed polarity in Hole 748B (104–111 mbsf) to Chron C12r (Fig. 8). This interpretation is verified by the LO of the calcareous nannofossil *Reticulofenestra umbilica* (N3) and by three $^{87}Sr/^{86}Sr$ ages (S4, S5, and S6), which all lie close to the correlation line in Fig. 8 and confirm that this reversed polarity interval represents Chron C12r. Harwood and Maruyama (1992) suggested that a hiatus may be present in Chron C12r because, compared to polarity intervals above and below, Chron C12r is relatively thin. However, no diatom zones (or subzones) are missing in this interval of Hole 748B (i.e. the *Rhizosolenia oligocaenica* 'a', 'b', and 'c' subzones are present). Alternatively, the thinness of this subchron might reflect slower sedimentation rates. Both possibilities are indicated in Fig. 8. The normal polarity interval below Chron C12r (111.61–115.57 mbsf) can be correlated with Chron C13n. As mentioned above, this interpretation is supported by identification of the initial peak of the Oi-1 $\delta^{18}O$ event at 115.09 mbsf in Hole 748B (Zachos et al., 1992), as well as by two $^{87}Sr/^{86}Sr$ ages (S7 and S8) (Table 2). A thin reversed polarity interval (0.14 m thick) is recorded near the base of Chron C13n in Hole 748B. This interval was affected by drilling disturbances and may not reflect geomagnetic field behaviour. It should be noted that our interpretation suggests that the LO of *Isthmolithus recurvus* occurs in the mid- to upper part of Chron C12r in Hole 744A, but in the lower part of C12r in Hole 748B (Table 1). This confirms the statement by Berggren et al. (1995) that it is 'one of the most inconsistent datums'.

The Eocene–Oligocene boundary occurs just below the base of Chron C13n (Cande and Kent, 1992, 1995; Berggren et al., 1995). The LO of the calcareous nannofossil *Reticulofenestra oamaruensis* occurs in the upper part of Chron C13r at 33.7 Ma (Berggren et al., 1995) and is indicative of the Eocene–Oligocene boundary.

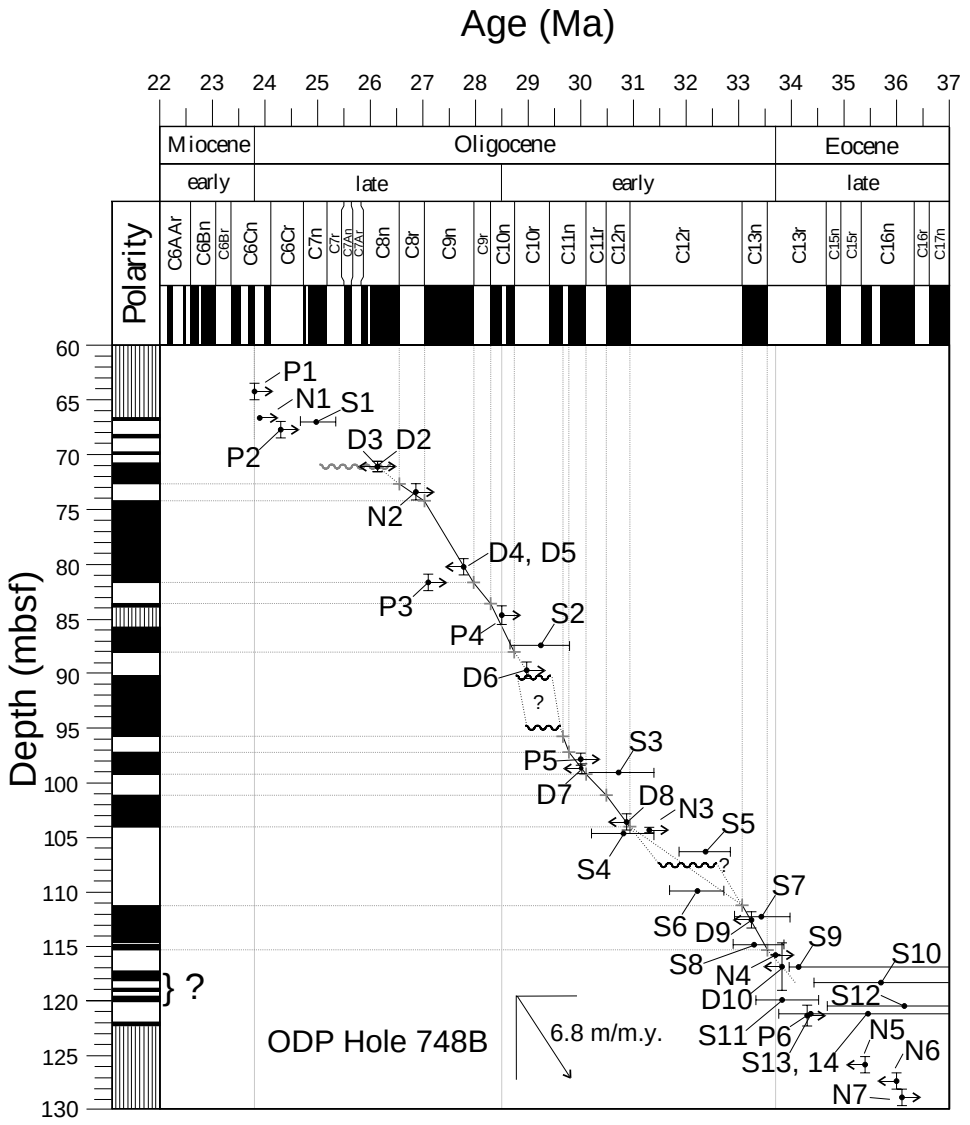

Fig. 8. Age versus depth plot with correlation of the Hole 748B polarity zonation to the GPTS of Cande and Kent (1995). Calcareous nannofossil (N) and planktonic foraminiferal (P) datums (from Berggren et al., 1995; Table 1) and $^{87}Sr/^{86}Sr$ (S) ages (from Zachos et al., 1999; Table 2) are used to constrain the interpretations. Diatom datums (D) are calibrated in this study and are shown on the correlation line at the depth where they occur in Hole 748B (Table 1). Age calibrations of the diatom datums are listed in Table 3. The question mark beside the thin normal polarity intervals at 117.5–120 mbsf indicates uncertainty due to the presence of two strong remanence components, which makes interpretation difficult. The question mark between 90 and 95 mbsf indicates uncertainty concerning the position of the inferred unconformity. $^{87}Sr/^{86}Sr$ ages S15, 16 and 17 (Table 2) are not shown for the sake of clarity: no correlation of the polarity pattern is made for the lower part of the studied interval.

This datum (N4) lies at 115.90 mbsf in Hole 748B, which agrees with our magnetostratigraphic interpretation. Below 122.51 mbsf, the intensity and stability of the magnetization decreases and determination of reliable ChRM directions becomes impossible. The interval between 117.5 and 120.5 mbsf contains several thin normal polarity zones (Fig. 5), which appear to make the polarity cor-

relation too old (based on downward extrapolation of sedimentation rates). The sediments from this interval contain at least two strong remanence components and it is not clear that the primary magnetization has been isolated for this interval. We therefore do not interpret the magnetic polarity record below ~117 mbsf for Hole 748B.

There is a one-to-one correlation between the magnetic polarity pattern in Hole 748B and the GPTS above Chron C12r, up to about 95 mbsf. We correlate the interval from ~95 to 104 mbsf to the base of Chron C11n.1n and to chrons C11n.1r, C11n.2n, C11r and C12n, respectively. The LO of *Subbotina angiporoides* (P5; see Berggren et al., 1995) at 97.95 mbsf and a $^{87}Sr/^{86}Sr$ date at 99.10 mbsf (S3) confirm this interpretation. Above ~95 mbsf, interpretation becomes more difficult. Based on biostratigraphic datums above and below the interval around 91–95 mbsf, and on the difficulty in matching the palaeomagnetic polarity pattern, a middle-Oligocene hiatus seems to be present, but no diatom zones are missing and it is difficult to define the position of this possible hiatus. In Fig. 8, we indicate an interval of uncertainty from 91 to 95 mbsf. Harwood and Maruyama (1992) plotted a hiatus at ~90 mbsf, based only on the magnetostratigraphic data of Inokuchi and Heider (1992). Our middle-Oligocene magnetostratigraphy for Hole 748B does not necessarily require a hiatus in this interval, although Chron C11n.1r does not appear to be recorded and Chron C10r would appear to be unusually thin. The presence of a hiatus therefore seems likely, but higher-resolution biostratigraphic sampling would be necessary to resolve the position of this inferred hiatus. Alternatively, it is possible that part of the stratigraphic succession was not recovered at the core break between cores 10H and 11H (Figs. 5,8).

Above this interval of uncertainty, interpretation of the polarity pattern recorded in Hole 748B is again reasonable between 71 and 90 mbsf. The thick interval of normal polarity between 74.2 and 81.94 mbsf probably correlates with Chron C9n, which is the longest normal polarity interval in the Oligocene (Fig. 8). Interpretation of the polarity zonation above and below Chron C9n is consistent with the LO of *Chiasmolithus altus* (N2), which should fall within Chron C8r (Berggren et al., 1995). Also, the LO of *C. cubensis* (P4) falls as it should within Chron C10n and the $^{87}Sr/^{86}Sr$ date at 87.50 mbsf (S2) is consistent with this interpretation. The thickness of this chron is exaggerated in Fig. 8 because of a coring gap at 84–86 mbsf (Fig. 5). The only significant problem with this correlation is that the LO of *Globigerina labiacrassata* (P3) occurs at the base of Chron C9n (81.75 mbsf) instead of at the top of C9n. However, this could be due to environmental factors.

The strongest biostratigraphic evidence for a hiatus in the studied interval of Hole 748B is in the uppermost Oligocene (70.61–71.58 mbsf). The *Rocella gelida* 'a' Subzone is missing at this level (and probably part of the *Lisitzinia ornata* Zone), as indicated by the concurrent LO of *R. vigilans* var. B (D2) and the FO of *R. gelida* (D3). The ages for these datums, however, are not robustly calibrated because they are based on previous calibrations from holes 744A and 748B. It is difficult to interpret the uppermost part of the studied section above this unconformity (60–70 mbsf). We show the biostratigraphic datums and a single $^{87}Sr/^{86}Sr$ age (S1) for this interval but refrain from interpreting the polarity signal. High-resolution palaeomagnetic analysis of core 8H would provide a better context for the magnetostratigraphic interpretation of the uppermost part of the interval studied here. It is worth noting that the LO of *L. ornata* (D1) occurs above the inferred upper Oligocene hiatus at 70.61–71.58 mbsf (Table 1) and below the LO of *Dictyococcites bisectus* (N1) and the LO of *Tenuitella gemma* (P2) (Fig. 8). There is no evidence for a hiatus between D1 and these other two datums. It is also worth noting that the LO of *Chiasmolithus altus* (N2) occurs in Chron C8r, which is consistent with its location at DSDP site 522 (Poore et al., 1982; Percival, 1984). Berggren et al. (1995) noted that this datum is located within Chron C8n in Hole 744A (Wei and Thierstein, 1991), which suggested that this datum is diachronous between low and mid latitudes. Our results indicate that this interval is difficult to interpret in Hole 744A, but clear identification of the LO of *C. altus* within Chron C8r

in Hole 748B indicates that this datum is not diachronous.

5.3. Calibration of Eocene–Oligocene diatom datums for the southern Kerguelen Plateau

By using calcareous nannofossil and planktonic foraminiferal biostratigraphy and Sr-isotope ages to constrain our interpretations of the magnetic polarity zonations for ODP holes 744A and 748B, we can now revise the calibration of diatom datums for the southern Kerguelen Plateau. The diatom datums documented by Baldauf and Barron (1991) and Harwood and Maruyama (1992) are listed in Table 1 and are shown on the correlation lines in Figs. 7 and 8. Where the age interpretation is clear, it is possible to calibrate the diatom datums (Table 3). Of the 10 datums recognised, four are clearly synchronous in both holes (FO *Lisitzinia ornata* (D4), FO *Rocella vigilans* var. B (D5), FO *Cavitatus jouseanus* (D8) and FO *Rhizosolenia oligocaenica* (D10)). The FO of *Rhizosolenia antarctica* (D9) is only reported in Hole 748B, therefore it is not possible to determine whether it is synchronous across the southern Kerguelen Plateau. It should be noted that we have observed *R. antarctica* in samples from Hole 744A, and, with further careful work, it should be possible to identify its FO and test whether it is synchronous with its position in Hole 748B. The three youngest datums fall so close to an unconformity in the middle of the late Oligocene that it is difficult to calibrate them (LO *L. ornata* (D1), LO *R. vigilans* var. B (D2), and FO *Rocella gelida* (D3)). Similarly, datums D6 (LCO *R. vigilans* var. A) and D7 (FO *R. vigilans* var. A) lie near the middle Oligocene unconformity in Hole 744A. However, despite uncertainty concerning the position of this unconformity (Fig. 7), it is possible that the positions of D6 and D7 are consistent in the two holes and that the ages obtained from Hole 748B are reliable. The ages listed in Table 3 are the best available estimates for these diatom datums from the southern Kerguelen Plateau based on the detailed revision of the magnetostratigraphy for holes 744A and 748B as presented in this study. It should be noted that Harwood and Maruyama (1992) suggested that *R. vigilans* had two separate northward migrations to the Kerguelen Plateau from southern waters (designated as var. A and B, respectively). If the LCO of *R. vigilans* var. A and the FO of *R. vigilans* var. B represent migration events, then these datums might not be synchronous in other parts of the Southern Ocean. They should therefore be used with caution, although their synchroneity across the Kerguelen Plateau indicates they are biostratigraphically useful in this region. We have therefore retained them in Table 3.

5.4. Erosion events

The southern Kerguelen Plateau lies just to the north of a constricted deep-water passage (Fig. 1) and would be expected to record erosive events associated with fluctuations of circumpolar deep water as it moved eastward around Antarctica. Available evidence suggests the presence of two significant unconformities in the studied intervals of holes 744A and 748B (Figs. 7 and 8). The chronology is difficult to interpret in the vicinity of the unconformities; however, the unconformities appear to be coeval in both holes.

In Hole 744A, the middle Oligocene unconformity has resulted in lack of sediment preservation (due either to erosion or non-deposition) between chrons C10n and C11r (~28.5–30.5 Ma), whereas in Hole 748B this unconformity seems to have resulted in loss of sediment around C10r and C11n.1n (~29.0–29.5 mbsf). The apparent longer duration of erosion/non-deposition at Site 744 may have resulted from its greater water depth, which would make it more prone to scouring by enhanced bottom water flow. A similar situation is evident in the Weddell Sea, where a coeval unconformity is present at Site 690 on the flanks of Maud Rise (water depth = 2914 m), but not near the crest of Maud Rise at Site 689 (water depth = 2080 m) (Spiess, 1990; Florindo and Roberts, unpublished data). There is also widespread evidence for middle Oligocene unconformities in the circum-Antarctic region, which date after the LO of *Subbotina angiporoides* at 30.0 Ma (P5; Table 1) and before the LO of *Chiloguembelina cubensis* at 28.5 Ma (P4; Table 1). These observa-

Table 3
Recalibration of Eocene–Oligocene diatom datums for the southern Kerguelen Plateau (this study)

	Hole 744A				Hole 748B				Southern Kerguelen Plateau		
	Average depth	±m	Age calibration	Chron	Average depth	±m	Age calibration	Chron	Designation	Synchronous?	Age
(mbsf)		(Ma)		(mbsf)		(Ma)					(Ma)
LO *Lisitzinia ornata*	105.06	0.75	~24.8	C7n?	69.60	0.48	?	?	D1	?	~24.8
LO *Rocella vigilans* var. B	105.06	0.75	~24.8	C7n?	71.10	0.48	=26.3	=C8n	D2	?	~24.8
FO *Rocella gelida*	106.56	0.75	27.1	C9n/C8r	71.10	0.48	=26.3	=C8n	D3	?	27.1
FO *Lisitzinia ornata*	110.06	0.75	27.8	C9n	80.33	0.75	27.8	C9n	D4	Yes	27.8
FO *Rocella vigilans* var. B	109.76	1.06	27.6	C9n	80.33	0.75	27.8	C9n	D5	Yes	27.8
LCO *Rocella vigilans* var. A	118.5	0.35	?	?	89.83	0.75	~29.0	C10r	D6	?	~29.0
FO *Rocella vigilans* var. A	119.58	0.73	?	?	98.85	0.27	30.0	C11n.2n	D7	?	30.0
FO *Cavitatus jouseanus*	124.06	0.75	30.8	C12n	103.83	0.75	30.9	C12n	D8	Yes	30.9
FO *Rhizosolenia antarctica*	–	–	–	–	112.52	0.75	33.2	C13n	D9	?	33.2
FO *Rhizosolenia oligocaenica*	147.35	0.15	33.6	C13r	116.86	2.22	33.8	C13r	D10	Yes	33.8

For details of age interpretations used for the calibration, see text and Figs. 7 and 8. For datums where there is a narrow range of ages between the two holes, the oldest age is used for FOs.

tions suggest that this erosion event marks the onset of the Antarctic circumpolar current (Carter and Landis, 1972; Kennett et al., 1972; Jenkins, 1974; Fulthorpe et al., 1996). A middle Oligocene date is coeval with opening of the Drake Passage at 31 ± 2 Ma (Lawver and Gahagan, 2003), which provides a strong link between tectonic opening of this deep ocean gateway and development of the Antarctic circumpolar current.

Holes 744A and 748B also contain evidence for an erosive event in the middle of the late Oligocene. The duration of this event is difficult to estimate because of the poorly constrained chronology immediately above the inferred unconformity. The oldest sediments below the unconformity appear to date between chrons C8n and C8r (Figs. 7 and 8). A marked unconformity is also evident at this time at sites 689 and 690 at Maud Rise (Spiess, 1990; Florindo and Roberts, unpublished data). By analogy with the middle Oligocene erosive event, it is possible that this unconformity is linked to a period of enhanced bottom water circulation.

5.5. Sedimentation rates

Inspection of the slope of the correlation lines in Figs. 7 and 8 indicates that sedimentation rates were low (~7 m/Myr), relatively uniform, and similar in both holes for much of the studied interval. This suggests that sedimentation processes were similar at the two sites. Both sites were situated above the CCD throughout the Eocene and Oligocene, and the majority of the sediment is biogenic in origin. The low sedimentation rates probably reflect low biological productivity. Despite the activity of bottom currents, which were probably responsible for the unconformities documented in both holes, it appears that deposition from bottom currents was not significant since the sedimentation rates were so low.

6. Conclusions

We have conducted high-resolution magnetostratigraphic studies of Eocene–Oligocene sediments from ODP holes 744A and 748B. For the

intervals where high-quality palaeomagnetic data are available, our results suggest that it is necessary to make minor to major revisions to the magnetic polarity zonations for both holes compared to previously published studies (Keating and Sakai, 1991; Inokuchi and Heider, 1992). The magnetizations are weaker in Hole 748B compared to Hole 744A and no robust palaeomagnetic signal was obtained for the Eocene in Hole 748B. Interpretation of the magnetic polarity zonation for both holes was constrained using calcareous nannofossil and planktonic foraminiferal biostratigraphic datums (Berggren et al., 1995), and using Sr-isotope ages (Barrera et al., 1991; Zachos et al., 1999). We have re-calibrated the diatom datums in these holes (Baldauf and Barron, 1991; Harwood and Maruyama, 1992) using our new integrated chronostratigraphic interpretations. With this calibration, it can be demonstrated that four diatom datums are synchronous across the southern Kerguelen Plateau, including the FO of *Lisitzinia ornata* (27.8 Ma), the FO of *Rocella vigilans* var. B (27.8 Ma), the FO of *Cavitatus jouseanus* (30.9 Ma) and the FO of *Rhizosolenia oligocaenica* (33.8 Ma). In addition, although the ages of some datums are obscured by an unconformity in Hole 744A, it is possible to use the age interpretation from Hole 748B to provide age estimates for the LCO of *R. vigilans* var. A (~29.0 Ma), the FO of *R. vigilans* var. A (30.0 Ma) and the FO of *Rhizosolenia antarctica* (33.2 Ma). Other diatom datums are poorly constrained in the two studied holes. The synchroneity of the diatom datums examined in this study suggests that diatom biostratigraphy has considerable promise for correlation in the Southern Ocean. Human factors and differences in approach and synthesis of data sets are more likely to be responsible for the diachronism noted by Ramsay and Baldauf (1999). Further careful assessment of Southern Ocean diatom datums is still required. It should also be noted that the last occurrence of the calcareous nannofossil *Chiasmolithus altus* occurs in Chron C8r rather than C8n in our revised magnetostratigraphic interpretation, which indicates that this datum is not diachronous between low and mid latitudes as had previously been suggested (Berggren et al., 1995). Two major erosive events are recorded in holes 744A and 748B in the middle Oligocene and in the middle of the late Oligocene, respectively. The earlier event appears to be related to development of the Antarctic circumpolar current, which appears to be coeval with tectonic opening of the Drake Passage. The later erosion event may also reflect a period of enhanced bottom water circulation.

Acknowledgements

We are grateful to Richard Weaver for help with sampling, Kevin Padley for technical assistance in the SOC palaeomagnetic laboratory, Matt Cooper for help with conversion of $^{87}Sr/^{86}Sr$ ages to the most recent Sr-isotope timescale and John Barron and Jim Channell for constructive reviews of the manuscript. We are also grateful to the ODP curatorial advisory board for granting permission to work on this valuable core material and to ODP personnel at the East Coast Repository at LDEO for their assistance with sampling. The ODP is sponsored by the US National Science Foundation (NSF) and participating countries (including the UK) under management of Joint Oceanographic Institutions (JOI), Inc. The SOC palaeomagnetic laboratory and this project were supported by grants from the UK NERC. A.P.R. gratefully acknowledges financial support from the Leverhulme Trust.

References

Baldauf, J.G., Barron, J.A., 1991. Diatom biostratigraphy: Kerguelen Plateau and Prydz Bay regions of the Southern Ocean. In: Barron, J., Larsen, B., et al. (Eds.), Proc. ODP Sci. Res. 119, 547–598.

Barrera, E., Barron, J., Halliday, A., 1991. Strontium isotope stratigraphy of the Oligocene-lower Miocene section at site 744, southern Indian Ocean. In: Barron, J., Larsen, B., et al. (Eds.), Proc. ODP Sci. Res. 119, 731–738.

Barron, J., Larsen, B., et al., 1989. Proc. ODP Init. Repts. 119.

Berggren, W.A., 1992. Paleogene planktonic foraminifer magnetobiostratigraphy of the Southern Kerguelen Plateau (Sites 747-749). In: Wise, S.W., Jr., Schlich, R., et al. (Eds.), Proc. ODP Sci. Res. 120, 551–568.

Berggren, W.A., Kent, D.V., Swisher, III, C.C., Aubry, M.-P., 1995. A revised Cenozoic geochronology and chronostratig-

raphy. In: Berggren, W.A., Kent, D.V., Aubry, M.-P., Hardenbol, J. (Eds.), Geochronology, Time Scales and Global Stratigraphic Correlation. SEPM Spec. Publ. 54, 129–212.

Bohaty, S.M., Harwood, D.M., 2000. Ebridian and silicoflagellate biostratigraphy from Eocene McMurdo erratics and the Southern Ocean. In: Stilwell, J.D., Feldmann, R.M. (Eds.), 2000. Paleobiology and Paleoenvironments of Eocene Rocks, McMurdo Sound, East Antarctica, Am. Geophys. Un. Ant. Res. Ser. 76, 99–159.

Bottomley, R., Grieve, R., York, D., Masaitis, V., 1997. The age of the Popigai impact event and its relation to events at the Eocene/Oligocene boundary. Nature 388, 365–368.

Cande, S.C., Kent, D.V., 1992. A new geomagnetic polarity time scale for the late Cretaceous and Cenozoic. J. Geophys. Res. 97, 13917–13951.

Cande, S.C., Kent, D.V., 1995. Revised calibration of the geomagnetic polarity time scale for the late Cretaceous and Cenozoic. J. Geophys. Res. 100, 6093–6095.

Carter, R.M., Landis, C.A., 1972. Correlative Oligocene unconformities in southern Australasia. Nat. Phys. Sci. 237, 12–13.

Chung, S.L., Lo, C.H., Lee, T.Y., Zhang, Y., Xie, Y., Li, X., Wang, K.L., Wang, P.L., 1998. Diachronous uplift of the Tibetan plateau starting 40 Myr ago. Nature 394, 769–773.

Coffin, M.F., Eldholm, O., 1994. Large igneous provinces: crustal structure, dimensions, and external consequences. Rev. Geophys. 32, 1–36.

Farley, K.A., Montanari, A., Shoemaker, E.M., Shoemaker, C.S., 1998. Geochemical evidence for a comet shower in the Late Eocene. Science 280, 1250–1253.

Fitzgerald, P.G., 1992. The Transantarctic Mountains of southern Victoria Land; the application of apatite fission track analysis to a rift shoulder uplift. Tectonics 11, 634–662.

Florindo, F., Wilson, G.S., Roberts, A.P., Sagnotti, L., Verosub, K.L., 2001. Magnetostratigraphy of late Eocene - early Oligocene glaciomarine sediments from the CRP-3 core, McMurdo Sound, Ross Sea, Antarctica. Terra Ant. 8, 599–613.

Florindo, F., Bohaty, S.M., Erwin, P.S., Richter, C., Roberts, A.P., Whalen, P.A., Whitehead, J.M., 2003. Magnetobiostratigraphic chronology and palaeoenvironmental history of Cenozoic sequences from ODP Sites 1165 and 1166, Prydz Bay, Antarctica. Palaeogeogr. Palaeoclimatol. Palaeoecol. (this issue) 10.1016/S0031-0182(03)00395-X

Fuller, M., Hastedt, M., Herr B., 1998. Coring-induced magnetization of recovered sediment. In: Weaver, P.P.E., Schmincke, H.-U., Firth, J.V., Duffield, W., et al. (Eds.), Proc. ODP Sci. Res. 157, 47–56.

Fulthorpe, C.S., Carter, R.M., Miller, K.G., Wilson, J., 1996. Marshall Paraconformity: a mid-Oligocene record of inception of the Antarctic Circumpolar Current and coeval glacio-eustatic lowstand? Mar. Petrol. Geol. 13, 61–77.

Gladczenko, T.P., Coffin, M.F., 2001. Kerguelen Plateau crustal structure and basin formation from seismic and gravity data. J. Geophys. Res. 106, 16583–16601.

Harwood, D.M., Maruyama, T., 1992. Middle Eocene to Pleistocene diatom biostratigraphy of ODP Leg 120, Kerguelen Plateau. In: Wise, S.W., Jr., Schlich, R., et al. (Eds.), Proc. ODP Sci. Res. 120, 683–733.

Harwood, D.M., Bohaty, S.M., Scherer, R.P., 1998. Lower Miocene diatom biostratigraphy of the CRP-1 drillcore, McMurdo Sound, Antarctica. Terra Ant. 5, 499–514.

Heider, F., Körner, U., Bitschene, P., 1993. Volcanic ash particles as carriers of remanent magnetization in deep-sea sediments from the Kerguelen Plateau. Earth Planet. Sci. Lett. 118, 121–134.

Huber, B.T., 1991. Paleogene and early Neogene planktonic foraminifera biostratigraphy of sites 738 and 744, Kerguelen Plateau (southern Indian Ocean). In: Barron, J., Larsen, B., et al. (Eds.), Proc. ODP Sci. Res. 119, 427–450.

Inokuchi, H., Heider, F., 1992. Magnetostratigraphy of sediments from sites 748 and 750, ODP Leg 120. In: Wise, S.W., Jr., Schlich, R., et al. (Eds.), Proc. ODP Sci. Res. 120, 247–252.

Jenkins, D.G., 1974. Initiation of the proto circum-Antarctic current. Nature 252, 371–373.

Keating, B.H., Sakai, H., 1991. Magnetostratigraphic studies of sediments from Site 744, southern Kerguelen Plateau. In: Barron, J., Larsen, B., et al. (Eds.), Proc. ODP Sci. Res. 119, 771–794.

Kennett, J.P., Burns, R.E., Andrews, J.E., Churkin, M., Jr., Davies, T.A., Dumitrica, P., Edwards, A.R., Galehouse, J.S., Packham, G.H., van der Lingen, G.J., 1972. Australian-Antarctic continental drift, palaeocirculation changes and Oligocene deep-sea erosion. Nat. Phys. Sci. 239, 51–55.

Kirschvink, J.L., 1980. The least-squares line and plane and the analysis of palaeomagnetic data. Geophys. J. R. Astron. Soc. 62, 699–718.

Koeberl, C., Poag, C.W., Reimold, W.U., Brandt, D., 1996. Impact origin of the Chesapeake Bay structure and the source of the North American tektites. Science 271, 1263–1266.

Kok, Y.S., Tauxe, L., 1996a. Saw-toothed pattern of relative paleointensity records and cumulative viscous remanence. Earth Planet. Sci. Lett. 137, 95–99.

Kok, Y.S., Tauxe, L., 1996b. Saw-toothed pattern of sedimentary paleointensity records explained by cumulative viscous remanence. Earth Planet. Sci. Lett. 144, E9–E14.

Lawver, L.A., Gahagan, L.M., Coffin, M.F., 1992. The development of paleoseaways around Antarctica. In: Kennett, J.P., Warnke, D.A. (Eds.), The Antarctic Paleoenvironment: A Perspective on Global Change, Part I. Am. Geophys. Un. Ant. Res. Ser. 56, 7–30.

Lawver, L.A., Gahagan, L.M., 2003. The evolution of Cenozoic seaways in the circum-Antarctic region. Palaeogeogr. Palaeoclimatol. Palaeoecol. (this issue) 10.1016/S0031-0182(03)00392-4

Mazaud, A., 1996. Sawtooth variation in magnetic profiles and delayed acquisition of magnetization in deep-sea cores. Earth Planet. Sci. Lett. 139, 379–386.

McArthur, J.M., Howarth, R.J., Bailey, T.R., 2001. Strontium

isotope stratigraphy: LOWESS version 3: Best fit to the marine Sr-isotope curve for 0-509 Ma and accompanying look-up table for deriving numerical age. J. Geol. 109, 155–170.

Munschy, M., Dyment, J., Boulanger, M.O., Boulanger, D., Tissot, J.D., Schlich, R., Rotstein, Y., Coffin, M.F., 1992. Breakup and seafloor spreading between the Kerguelen Plateau - Labuan Basin and the Broken Ridge - Diamantina Zone. In: Wise, S.W., Jr., Schlich, R., et al. (Eds.), Proc. ODP Sci. Res. 120, 931–944.

O'Brien, P.E., Cooper, A.K., Richter, C., et al., 2001. Proc. ODP Init. Repts. 188.

Opdyke, N.D., Channell, J.E.T., 1996. Magnetic Stratigraphy. Academic Press, San Diego, CA, 346 pp.

Pearson, P.N., Palmer, M.R., 2000. Atmospheric carbon dioxide concentrations over the past 60 million years. Nature 406, 695–699.

Percival, S.F., 1984. Late Cretaceous to Pleistocene calcareous nannofossils from the South Atlantic, Deep Sea Drilling Project 73. Init. Repts. DSDP 73, 391–424.

Poore, R.Z., Tauxe, L., Percival, S.F., LaBrecque, J.L., 1982. Late Eocene-Oligocene magnetostratigraphy and biostratigraphy at South Atlantic DSDP Site 522. Geology 10, 508–511.

Ramsay, A.T.S., Baldauf, J.G., 1999. A reassessment of the Southern Ocean biochronology. Geol. Soc. Lond. Mem. 18, 122 pp.

Raymo, M.E., Ruddiman, W.F., 1992. Tectonic forcing of late Cenozoic climate. Nature 359, 117–122.

Roberts, A.P., Stoner, J.S., Richter C., 1996. Coring-induced magnetic overprints and limitations of the long-core paleomagnetic measurement technique: some observations from ODP Leg 160, Eastern Mediterranean Sea. In: Emeis, K.C., Robertson, A.H.F., Richter, C., et al. (Eds.), Proc. ODP Init. Repts. 160, 497–505.

Roberts, A.P., Wilson, G.S., Florindo, F., Sagnotti, L., Verosub, K.L., Harwood, D.M., 1998. Magnetostratigraphy of lower Miocene strata from the CRP-1 core, McMurdo Sound, Ross Sea, Antarctica. Terra Ant. 5, 703–713.

Ruddiman, W.F., Kutzbach, J.E., 1989. Forcing of late Cenozoic Northern Hemisphere climate by plateau uplift in southern Asia and the American west. J. Geophys. Res. 94, 18409–18427.

Schlich, R., Wise, S.W., Jr., et al., 1989. Proc. ODP Init. Repts. 120.

Spiess, V., 1990. Cenozoic magnetostratigraphy of Leg 113 drill sites, Maud Rise, Weddell Sea, Antarctica. In: Barker, P.F., Kennett, J.P., et al. (Eds.), Proc. ODP Init. Repts. 113, 261–315.

Stokking, L.B., Musgrave, R.J., Bontempo, D., Autio, W., 1993. Handbook for shipboard paleomagnetists. Texas A&M Univ. Tech. Note 18, College Station, TX (Ocean Drilling Program), 148 pp.

Tikku, A.A., Cande, S.C., 2000. On the fit of Broken Ridge and Kerguelen Plateau. Earth Planet. Sci. Lett. 180, 117–132.

Vonhof, H.B., Smit, J., Brinkhuis, H., Montanari, A., Nederbragt, A.J., 2000. Global cooling accelerated by early late Eocene impacts? Geology 28, 687–690.

Weeks, R., Laj, C., Endignoux, L., Fuller, M., Roberts, A., Manganne, R., Blanchard, E., Goree, W., 1993. Improvements in long core measurement techniques: applications in palaeomagnetism and palaeoceanography. Geophys. J. Int. 114, 651–662.

Wei, W., Thierstein, H., 1991. Upper Cretaceous and Cenozoic calcareous nannofossils of the Kerguelen Plateau (southern Indian Ocean) and Prydz Bay (East Antarctica). In: Barron, J., Larsen, B., et al. (Eds.), Proc. ODP Sci. Res. 119, 467–493.

Wei, W., Wise, S.W., Jr., 1992. Oligocene-Pleistocene calcareous nannofossils from Southern Ocean Sites 747, 748 and 751. In: Wise, S.W., Jr., Schlich, R., et al. (Eds.), Proc. ODP Sci. Res. 120, 509–521.

Wei, W., Villa, G., Wise, S.W., Jr., 1992. Paleoceanographic implications of Eocene-Oligocene calcareous nannofossils from Sites 711 and 748 in the Indian Ocean. In: Wise, S.W., Jr., Schlich, R., et al. (Eds.), Proc. ODP Sci. Res. 120, 979–999.

Wilson, G.S., Roberts, A.P., Verosub, K.L., Florindo, F., Sagnotti, L., 1998. Magnetobiostratigraphic chronology of the Eocene-Oligocene transition in the CIROS-1 core, Victoria Land margin, Antarctica: implications for Antarctic glacial history. Geol. Soc. Am. Bull. 110, 35–47.

Wilson, G.S., Bohaty, S.M., Fielding, C.R., Florindo, F., Hannah, M.J., Harwood, D.M., McIntosh, W.C., Naish, T.R., Roberts, A.P., Sagnotti, L., Scherer, R.P., Strong, C.P., Verosub, K.L., Villa, G., Watkins, D.K., Webb, P.-N., Woolfe, K.J., 2000. Chronostratigraphy of the CRP-2/2A drillhole, Ross Sea, Antarctica. Terra Ant. 7, 647–655.

Zachos, J.C., Berggren, W.A., Aubry, M.-P., Mackensen, A., 1992. Isotope and trace element geochemistry of Eocene and Oligocene foraminifers from site 748, Kerguelen Plateau. In: Wise, S.W., Jr., Schlich, R., et al. (Eds.), Proc. ODP Sci. Res. 120, 839–854.

Zachos, J.C., Opdyke, B.N., Quinn, T.M., Jones, C.E., Halliday, A.N., 1999. Early Cenzoic glaciation, Antarctic weathering, and seawater $^{87}Sr/^{86}Sr$: is there a link? Chem. Geol. 161, 165–180.

Zachos, J.C., Quinn, T.M., Salamy, K.A., 1996. High-resolution (10^4 years) deep-sea foraminiferal stable isotope records of the Eocene-Oligocene climate transition. Paleoceanography 11, 251–266.